Electrophoretic maneuvering of nonuniformly charged particles suspended in linear flows: Impact of the medium viscoelasticity

Rajnandan Borthakur* and Uddipta Ghosh†
Department of Mechanical Engineering, Indian Institute of Technology Gandhinagar, Palaj 382355, Gujarat, India

(Received 2 October 2023; accepted 8 January 2024; published 13 February 2024)

Electrophoresis in complex (non-Newtonian) fluidic media is becoming increasingly prominent owing to its applications in a wide variety of separation processes. Although most particles that undergo electrophoresis carry nonuniform surface charge, their motion in complex fluidic media has been addressed only recently, while many other separation processes also use externally imposed flows. Despite this, the impact of external flows on the electrophoretic motion of such particles in non-Newtonian fluids still remains largely unexplored. To address this, here we develop a semianalytical framework using a combination of matched asymptotic expansion and regular perturbation to examine the trajectories of nonuniformly charged particles suspended in a viscoelastic medium, subject to imposed shear flow and electric field. We assume the particle's surface charge to be weak but otherwise arbitrary, the electrical double layer to be thin, the suspending medium to obey the Oldroyd-B constitutive relation, and the overall flow to be weakly viscoelastic. Our results reveal that in the presence of imposed flows, any particle carrying a nonuniform surface charge will likely undergo cross-stream migration when the suspending medium is viscoelastic. It is shown that the very nature of a particle's trajectory and the extent of its migration will strongly depend on whether the imposed flow or the electrophoretic propulsion dominates particle motion. This is further supported by a reduced order model derived for Newtonian fluids, using which particles' velocities and their trajectories may be deduced without a detailed knowledge of the flow field. We demonstrate that in the limit of weak viscoelasticity, the general conclusions from this reduced order model may indeed be extended beyond the realm of Newtonian fluids. Our framework may be useful towards improving particle separation relevant to many biochemical applications.

DOI: 10.1103/PhysRevFluids.9.023302

I. INTRODUCTION

Electrophoresis, defined as the movement of charged particles through a fluid under the application of external electric fields [1–12], has long been a prominent area of research owing to its diverse applications starting from particle separation and sorting [13,14] to medical diagnostics [15–18]. For instance, capillary electrophoresis is widely used in commercial devices [17–19] to separate cells, DNA fragments, and the like for the purposes of sample detection. A somewhat related (albeit lesser known) technique, known as free flow electrophoresis (FFE) [14,20], employs a pressure-driven background flow in conjunction with an external electric field to continuously separate particles depending on their size and electric charge. FFE has been shown [21] to be particularly useful in sample purification and online monitoring when integrated with microfluidic platforms. Although

*rajnandanb@iitgn.ac.in
†uddipta.ghosh@iitgn.ac.in

there exists a rich body of literature on electrophoretic motion of charged colloidal particles, starting from the historical works of Smoluchowski [22] and Debye and Hückel [23] and later complemented by several others [1–6,24–28], the impact of externally imposed flows, like the ones encountered in FFE, on electrophoresis is rarely addressed in these studies. One possible reason for this stems from the fact that most previous studies with a few notable exceptions [2,8,29] exclusively focus on electrophoretic motion of uniformly charged particles in Newtonian fluids (such as electrolyte water solutions), wherein the impact of any background flow may be linearly superimposed with phoretic movement simply because the equations governing the flow are linear [30] on account of low Reynolds number. However, this linear superposition loses validity (as we shall show here) if the particle's surface charge becomes nonuniform or the suspending medium exhibits nonlinear constitutive behavior.

Colloidal particles bearing nonuniform surface charge density are commonplace in many applications. Indeed, variations in the surface charge either may occur naturally as found in proteins and DNA fragments as well as cells [2,31], or may also be intentionally engineered for specific applications, as done in the case of "Janus particles" [32,33]. Electrophoretic motion of nonuniformly charged particles in a Newtonian medium was first addressed by Anderson and co-workers [2,29], who established that the resulting particle velocities may be very elegantly expressed by adding the contributions from the multipole moments of the particle's surface charge. For instance, Anderson showed that the monopole moment results in translation, and the dipole moment causes rotation, while the quadrupole moment leads to cross-stream migration of the particle.

However, in many applications that involve electrophoresis, the suspending medium is non-Newtonian [34–38]. As an example, one may note that cross-linked polymer gels (such as polyacrylamide gels) are routinely used as the suspending medium for electrophoretic manoeuvring of colloidal particles [16]. At the same time, electrokinetic motion (so-called electroosmosis) of biologically relevant complex fluids such as plasma and blood in small-scale devices is also becoming increasingly prominent [39–42] for its relevance to medical diagnostic applications. As such, electrophoresis in non-Newtonian fluids has gained traction in the recent literature [7,34,36,43], wherein a handful of authors [34,44,45] have computed particle velocities using Carreau-type constitutive models, while during the last few years electrophoretic motion in viscoelastic medium has also been probed [7,36]. Li and Koch [36] estimated the electrophoretic velocity of a uniformly charged colloidal particle in a viscoelastic medium and showed that unlike Newtonian fluids, the particle velocity depends on its size even in the limit of a thin electrical double layer (EDL). Khair and Kabarowski [46] showed that a combination of an imposed shear flow and electrophoretic actuation may lead to cross-stream particle migration in a viscoelastic (second-order fluid) medium, although their results were later corrected by Choudhary *et al.* [47]. In another similar work Choudhary *et al.* [37] also reached a similar conclusion when they investigated the motion of uniformly charged particles driven by an electric field, suspended in a Poiseuille flow. More recently, Borthakur and Ghosh [8] have developed a generalized model for computing the electrophoretic velocity of a nonuniformly charged particle in an Oldroyd-B medium and showed that the variability in the surface charge, coupled with the nonlinear constitution of the suspending medium, also increases the particles' propensity for cross-stream migration, while the direction of their motion depends on their size as well as the multipole moments of the surface charge.

Despite the efforts outlined as above, electrophoretic motion of nonuniformly charged particles subject to externally imposed flows in a viscoelastic medium still remains an open question, with clear relevance to applications such as the free flow electrophoresis. In the absence of any external flow, the rotation of a nonuniformly charged particle eventually stops irrespective of the suspending fluid, when its dipole moment orients itself along the applied electric field [8], after which the particle simply follows a straight trajectory. However, a background flow with nonzero vorticity will inevitably induce its own angular velocity, which may aid or oppose the rotation caused by the nonuniform surface charge. This interaction, coupled with the nonlinear rheology of the medium, may indeed lead to nontrivial particle trajectories, which may be exploited to further improve separation, sorting, and detection processes.

In this article we thus aim to construct a semianalytical asymptotic framework to analyze electrophoretic trajectories of particles carrying arbitrary nonuniform surface charge, suspended in a viscoelastic fluid, subject to an externally imposed linear (shear) flow. The particle's surface charge is assumed to be weak, while the fluid's constitutive property is governed by the Oldroyd-B model [7,48]. Further, the EDL surrounding the particle is assumed to be thin, and we confine ourselves only to weakly viscoelastic flows. The asymptotic formulation is based upon a combination of singular and regular perturbation. First, we use matched asymptotic expansion to derive an expression for the modified Smoluchowski slip velocity [7] pertaining to the thin EDL limit. This is subsequently used in combination with the Lamb's general solution [49] and the generalized reciprocal theorem [50,51] to compute the angular and the translational velocities of the particle and later its trajectory in the suspending medium. We establish that for the special case of Newtonian fluids, particle trajectories may be computed by simply solving a set of ordinary differential equations (ODEs) without a detailed knowledge of the velocity field. This same framework also turns out to be useful in understanding particle motion when the suspending medium is viscoelastic. Our results demonstrate that the particle's angular and translational velocities as well as its trajectories exhibit qualitatively different trends depending on whether electrophoresis or the external flow dominates locally around the particle. In general, we show that the impact of a particle's size on its velocity and trajectory gets enhanced in the presence of a background flow.

The rest of this article proceeds as follows. We begin with the problem statement, the key assumptions, the elementary governing equations, and the asymptotic framework in Sec. II. The solutions to the particle velocities are discussed in Sec. III. Section IV outlines the numerical procedure adopted to compute the particle trajectories. The reduced order model for the special case of Newtonian fluids, along with a few representative results for particle trajectories in viscoelastic media, are included in Sec. V. In Sec. VI we compare some of our results with available experimental data from the literature and discuss a prospective experimental setup to test the predictions of this work. Finally, we conclude in Sec. VII.

II. THE PROBLEM STATEMENT

A. Physical description of the system

We consider a rigid nonconducting spherical particle of radius a bearing an arbitrary nonuniform charge density $\sigma'(\theta, \phi)$ on its surface (see Fig. 1), where θ and ϕ are respectively the polar and the azimuthal angles measured with respect to the direction of the flow. The particle is suspended in a viscoelastic fluid whose constitutive behavior in governed by the Olyroyd-B model [48]. This particular constitutive model is chosen such that the problem remains amenable to analytical treatment, yet without sacrificing the essential physics of viscoelastic contributions to particle motion. Indeed, the Oldroyd-B model, which is not without its limitations, does capture various key rheological features of polymeric fluids, such as the relaxation timescales, normal stress coefficients, etc., and has been shown [48] to be particularly useful for weakly viscoelastic flows considered in this article. The suspending medium has viscosity μ, permittivity ϵ, relaxation time λ_1', and retardation time λ_2' [48]. The electrolyte present in the fluid (bulk concentration c_0') dissociates into its constitutive ions and forms an EDL around the particle, as also shown in the figure.

We shall use three sets of axes to carry out the subsequent analysis. The first is the *laboratory-fixed axis* (r', θ, ϕ or, x', y', z', shown in green in Fig. 1), which will be used to track the particle's pathway. The second is the *body-fixed axis* ($\tilde{r}'$, $\tilde{\theta}$, $\tilde{\phi}$ or $\tilde{x}'$, $\tilde{y}'$, $\tilde{z}'$; see the schematic), which is attached to the particle's center of mass and rotates and translates with it. The third is the *central axis* ($\bar{r}'$, $\bar{\theta}$, $\bar{\phi}$ or, $\bar{x}'$, $\bar{y}'$, $\bar{z}'$; see Fig. 1), which at any given instant is stationary (like the laboratory-fixed axis) with its origin coinciding with the particle center. The central and the laboratory-fixed axes are always oriented along the same direction and hence have identical unit vectors. Initially (at $t' = 0$), the body-fixed axis and the central axis coincide with each other, unless otherwise mentioned. Therefore, the coordinates in these two axes are related as $\bar{\mathbf{x}} = \mathbf{x} - \mathbf{x}_P(t)$,

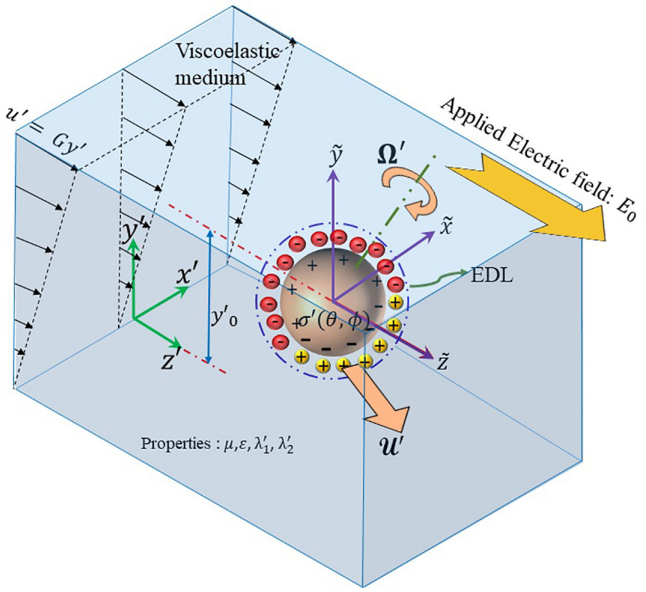

FIG. 1. Schematic of a spherical particle of radius a carrying arbitrary surface charge density $\sigma'(\bar{\theta}, \bar{\phi})$, suspended in a shear flow ($\mathbf{v}_\infty = Gy'\hat{\mathbf{e}}_z$) and subject to an electric field $E_0\hat{\mathbf{e}}_z$. The particle translates with velocity $\boldsymbol{\mathcal{U}}'$ and rotates with angular velocity $\boldsymbol{\Omega}'$. The surrounding medium is viscoelastic with viscosity μ, permittivity ϵ, relaxation time λ'_1, and retardation time λ'_2 and obeys the Oldroyd-B constitutive relation. The *laboratory-fixed*, *central*, and body-fixed axes are shown. The central and the body-fixed axes are assumed to coincide at $t = 0$.

where $\mathbf{x}_P(t)$ is the particle's position at time t measured in the laboratory-fixed axis. The purpose of defining three separate axes will become clear as we move on to compute the particle velocity in the forthcoming sections.

A steady electric field of magnitude E_0 (at $\bar{r} \to \infty$) is imposed along the z direction to move the particle electrophoretically. At the same time, it is also subject to a steady linear (shear) background flow with a far-field velocity, $\mathbf{v}'_\infty = Gy'\hat{\mathbf{e}}_z$ (see Fig. 1), where G is the imposed strain rate. We shall assume that initially the particle is located at $\mathbf{x}' = y'_0\hat{\mathbf{e}}_y$ in the laboratory-fixed axis, i.e., it has an initial offset of y'_0 along with y' axis. Note that in applications such as FFE, the imposed flow and the electric field do not always act along the same direction, as is the case here. Therefore, the system under consideration represents a somewhat simplified scenario, which nevertheless helps shed light on how electrophoretic motion and externally imposed flows interact with each other. The framework presented here may indeed be extended to scenarios where the imposed flow and the applied electric field are not colinear, akin to the applications mentioned as above; this we leave as a scope for future work.

Because of the background flow and the imposed electric field, the particle in general will undergo both translational and rotational motion. We assume the instantaneous translational velocity of the particle to be $\boldsymbol{\mathcal{U}}'(t')$, while its instantaneous angular velocity is denoted by $\boldsymbol{\Omega}'(t')$. Both of these velocities are *a priori* unknown and will be determined as part of the solution. The rotation of the particle will cause the charge density $[\sigma'(\theta, \phi)]$ to evolve with time in the laboratory-fixed as well as the central axes, which in turn will dictate its angular as well as translational velocities. At the same time, the translational velocity $[\boldsymbol{\mathcal{U}}'(t')]$ of the particle will govern its cross-stream migration, thus changing its position with respect to the imposed flow, which will subsequently impact the z component of the particle's velocity. This nontrivial coupling between the particle's surface charge, angular and translational velocities, and position with respect to the background flow may indeed

TABLE I. Characteristic scales chosen [1,52,53] to nondimensionalize pertinent variables, equations, and boundary conditions.

Quantity	Characteristic Scale	Remarks
Length	$r_c = a$	Particle radius
Ionic concentration	c_0'	Bulk concentration
Surface charge	σ_c	Known quantity
Surface potential	$\zeta_c = \sigma_c \lambda_D / \epsilon$	Debye length: $\lambda_D = \sqrt{\epsilon kT/2c_0' e^2}$
EDL potential	$\varphi_c = \zeta_c$	–
External potential	$\psi_c = E_0 a$	–
Velocity	$u_c = u_S = Ga$	Characteristic far-field velocity
Pressure and stresses	$p_c, \tau_c = \mu u_c / a$	–
Relaxation time	$\lambda_c = \lambda_1'$	Usually, $\lambda_1' > \lambda_2'$

lead to fascinating trajectories, as discussed in this article. It is worth noting at this point that in the body-fixed axis, the particle's surface charge distribution $[\sigma'(\tilde{\theta}, \tilde{\phi})]$ remains invariant with time.

B. The characteristic scales

We shall directly start with dimensionless variables for brevity as well as the convenience of analysis. To this end, the nondimensional version of any variable, say, ξ', is expressed as $\xi = \xi'/\xi_c$, where ξ_c is the characteristic value of the said variable. Table I outlines the characteristic scales chosen for all the relevant quantities. While most of these scales are trivial and have been extensively used by other researchers [1,7,54], it is nevertheless important to focus on two particular choices. First, we assume the characteristic surface charge density to be σ_c such that, $\sigma'(\bar{\theta}, \bar{\phi}) \sim O(\sigma_c)$. Based on this, we have further defined a characteristic surface potential (ζ_c), which quantifies the typical order of magnitude of the "zeta potential" on the particle surface. When the surface charge is uniform [say, $\sigma'(\bar{\theta}, \bar{\phi}) = \sigma_0'$], we may trivially choose $\sigma_c = \sigma_0'$. On the other hand, for a variable $\sigma'(\bar{\theta}, \bar{\phi})$, its surface average may be chosen as σ_c. Second, in the present scenario, there are two distinct velocity scales, namely, the characteristic electrophoretic velocity of the particle, $u_E = \epsilon \zeta_c E_0 / \mu$, and the characteristic imposed velocity, $u_S = Ga$. Table I shows that the latter (i.e., u_S) has been chosen as the velocity scale.

Enforcing the nondimensional variables defined using the characteristic scales as shown in Table I, several nondimensional numbers appear in the subsequent analysis and are listed in Table II. Of particular interest to us is the Deborah number (De), which quantifies the relative strength of the medium's viscoelasticity, and α, whose magnitude indicates the strength of electrophoretic motion relative to the imposed flow. Thus, $\alpha \ll 1$ will indicate a dominant imposed flow; $\alpha \gg \alpha_{\text{cr}}$ (defined

TABLE II. Various nondimensional numbers [1,7,48,52] that are relevant to the present analysis. D is the ionic diffusivity.

Quantity	Symbol	Expression
Ionic Péclet number	Pe	$u_c a / D$
EDL thickness	δ	λ_D / a
Char. surface potential w.r.t. thermal potential	$\bar{\zeta}_0$	$e\zeta_c / kT$
External field strength w.r.t. thermal potential	β	$eE_0 a / kT$
Ratio of the u_E to u_S	α	u_E / u_S
Deborah number	De	$u_c \lambda_c / a = G\lambda_1$
Initial offset of the particle	y_0	–

later) leads to electrophoresis controlling the particle motion, and $\alpha \sim O(1)$ means that both electrophoresis and the imposed flow play important roles in controlling the particle's movement.

C. The key assumptions

It is necessary to make a few assumptions in order to tackle the governing equations (discussed later) semianalytically. Although these assumptions simplify the equations, the essential physics of the problem is indeed preserved. We discuss the key ones among them below.

First, the EDL is assumed to be thin, which implies $\delta \ll 1$; this condition is indeed met in most practical applications [54]. Second, we assume the particle's surface charge density to be weak, which mandates $\bar{\zeta}_0 \ll 1$ [7]. Third, we consider the suspending medium to be weakly viscoelastic, which necessitates $\mathrm{De} \ll 1$. Fourth, the flow field is assumed to be quasisteady, which implies that the timescale associated with the evolving surface charge distribution is large compared to the relaxation timescale of the fluid itself [8]. Recall that the characteristic angular velocity of the particle is $\Omega_c \sim u_c/a \sim G$ and hence the quasisteady assumption will be satisfied if $\Omega_c^{-1} \gg \lambda_1'$, which leads to $\mathrm{De} \ll 1$, and this is consistent with the third assumption. Fifth, the presence of a depletion layer around the particle is ignored in our analysis, as is routinely done in the literature [36,37,55,56], and hence the entire fluid medium is assumed to obey the Oldroyd-B constitutive relation. Finally, we confine our attention to the low Reynolds number regime ($\mathrm{Re} \sim \rho_d u_c a/\mu \ll 1$, ρ_d is the fluid's density), which implies a viscosity dominated flow field.

D. Mathematical description of the problem

1. The fundamental equations

Here we shall lay out the fundamental equations that govern the particle's instantaneous angular and translational velocities, for a given charge distribution $[\sigma(\bar{\theta}, \bar{\phi})]$ on its surface. The flow around the particle is governed by the Poisson-Nernst-Planck-Cauchy momentum equations [1,48], coupled with the continuity equation for mass conservation and the Olyroyd-B constitutive model. As noted earlier, we shall directly start with the dimensionless versions of the above equations. In what follows, the total potential (Φ') has been split as $\Phi' = \psi' + \varphi'$, where ψ' is the externally imposed potential due to the applied electric field and is independent of the conditions on the particle's surface. φ' accounts for the contributions from the particle's surface charge and the EDL surrounding it. Note that these two components of the potential Φ' have two distinct characteristic scales as shown in Table I, such that ψ and φ are both $O(1)$ close to the particle.

For convenience, the Nernst-Planck equations are reformulated in terms of the salt concentration, $c = c_+ + c_-$ and the net charge density, $\rho = c_+ - c_-$ [7,57], where $c_{+(-)}$ is the concentration of positive (negative) ions present in the electrolyte. It may then be shown [1,54] that in the limit of weak surface charge, $\rho \sim O(\bar{\zeta}_0)$, and hence we may define $\tilde{\rho} = \rho/\bar{\zeta}_0$ such that $\tilde{\rho} \sim O(1)$. Now, using the nondimensionalization scheme stated in Sec. II B, the characteristic scales outlined in Table I, and the change of variables as discussed above, the governing equations take the following form:

$$\mathrm{Pe}(\mathbf{v} \cdot \nabla c) = \nabla \cdot \left(\nabla c + \bar{\zeta}_0 \beta \tilde{\rho} \nabla \psi + \bar{\zeta}_0^2 \tilde{\rho} \nabla \varphi\right), \tag{1a}$$

$$\mathrm{Pe}(\bar{\zeta}_0 \mathbf{v} \cdot \nabla \tilde{\rho}) = \nabla \cdot (\bar{\zeta}_0 \nabla \tilde{\rho} + \beta c \nabla \psi + \bar{\zeta}_0 c \nabla \varphi), \tag{1b}$$

$$\nabla^2 \psi = 0 \ \text{ and } \ \delta^2 \nabla^2 \varphi = \frac{-\tilde{\rho}}{2}, \tag{1c}$$

$$-\nabla p + \nabla \cdot \boldsymbol{\tau} + \alpha \nabla^2 \varphi \nabla \psi + \frac{\alpha \bar{\zeta}_0}{\beta} \nabla^2 \varphi \nabla \varphi = 0 \ \text{ and } \ \nabla \cdot \mathbf{v} = 0, \tag{1d}$$

$$\boldsymbol{\tau} + De \boldsymbol{\mathcal{T}} = 2\mathbf{D} + 2\lambda_2 De \boldsymbol{\mathcal{S}}, \tag{1e}$$

where p is the pressure, $\mathbf{v}$ is the velocity field, $\boldsymbol{\tau}$ is the deviatoric stress tensor, $\mathbf{D}$ is the strain rate tensor, and $\mathcal{T}$ and $\mathcal{S}$ are respectively the upper convected derivatives [48] of the stress tensor $\boldsymbol{\tau}$ and the strain rate tensor $\mathbf{D}$. The upper-convected derivative of a second rank tensor $\mathbf{A}$ may be written as $\mathbf{B} = \frac{\partial \mathbf{A}}{\partial t} + \mathbf{v}\cdot\nabla\mathbf{A} - (\nabla\mathbf{v})^T\cdot\mathbf{A} - \mathbf{A}\cdot(\nabla\mathbf{v})$. The detailed expressions for the various components of the convected derivatives may be found in Ref. [8]. The above equations are subject to the following boundary conditions, when expressed w.r.t. the *central axis*:

$$\hat{\mathbf{e}}_{\bar{r}}\cdot\left(-\nabla c + \mathrm{Pe}c\mathbf{v} - \bar{\zeta}_0^2\tilde{\rho}\nabla\varphi - \beta\bar{\zeta}_0\tilde{\rho}\nabla\psi\right)\big|_{\bar{r}=1} = 0, \tag{2a}$$

$$\hat{\mathbf{e}}_{\bar{r}}\cdot(-\bar{\zeta}_0\nabla\tilde{\rho} + \mathrm{Pe}\bar{\zeta}_0\tilde{\rho}\mathbf{v} - \bar{\zeta}_0 c\nabla\varphi - \beta c\nabla\psi)|_{\bar{r}=1} = 0, \tag{2b}$$

$$\nabla\psi\cdot\hat{\mathbf{e}}_{\bar{r}}|_{\bar{r}=1} = 0, \;\; \nabla\varphi\cdot\hat{\mathbf{e}}_{\bar{r}}|_{\bar{r}=1} = -\frac{\breve{\zeta}(\bar{\theta},\bar{\phi})}{\delta}, \tag{2c}$$

$$\mathbf{v}(\bar{r}=1,\bar{\theta},\bar{\phi}) = \boldsymbol{\Omega}\times\hat{\mathbf{e}}_{\bar{r}} + \boldsymbol{\mathcal{U}}, \tag{2d}$$

$$\varphi|_{\bar{r}\to\infty} = 0, \;\; \nabla\psi|_{\bar{r}\to\infty} = -\hat{\mathbf{e}}_z, \tag{2e}$$

$$\mathbf{v}\to\mathbf{v}_\infty = (\bar{y}+y_0)\hat{\mathbf{e}}_z, \quad c\to 2 \;\; \text{and} \;\; \tilde{\rho}\to 0, \;\; \text{as} \;\; \bar{r}\to\infty. \tag{2f}$$

In Eq. (2c), $\breve{\zeta}(\bar{\theta},\bar{\phi}) = \sigma'(\bar{\theta},\bar{\phi})/\sigma_c$ is analogous to the nondimensional zeta potential at the particle surface; since $\sigma' \sim O(\sigma_c)$, it follows that $\breve{\zeta}\sim O(1)$. Recall that the Cartesian unit vectors (i.e., $\hat{\mathbf{e}}_x$, $\hat{\mathbf{e}}_y$, and $\hat{\mathbf{e}}_z$) are identical in the central as well as the laboratory-fixed axes.

The particle velocities $\boldsymbol{\Omega}$ and $\boldsymbol{\mathcal{U}}$ are to be evaluated by carrying out a force and moment balance (about the particle's center) on the particle. It may be shown [8,58,59] that in the limit of thin EDL ($\delta \ll 1$), these two conditions may be respectively written as

$$\int_{S_p}(-p\boldsymbol{I}+\boldsymbol{\tau})\cdot\hat{\mathbf{e}}_{\bar{r}}\,dS = 0 \;\; \text{and} \;\; \int_{S_p}\hat{\mathbf{e}}_{\bar{r}}\times(\boldsymbol{\tau}\cdot\hat{\mathbf{e}}_{\bar{r}})\,dS = 0, \tag{3}$$

where the integration is carried out over the particle surface (S_p). The externally imposed potential (ψ) may be evaluated by solving Eq. (1c) subject to (2c) and (2e), which yields

$$\psi = -\left(\bar{r}+\frac{1}{2\bar{r}^2}\right)P_1(\eta), \tag{4}$$

where $\eta = \cos(\bar{\theta})$ and $P_1(\eta)$ is the Legendre polynomial of the first kind and order 1. We would like to clarify that the above solution has been expressed w.r.t. the central axis, with its origin located at the particle center.

2. The asymptotic limit of thin EDL, weak viscoelasticity, and weak surface charge

From Eq. (1c), it is evident that the thin EDL limit leads to a singular perturbation problem [7,60], which requires the use of matched asymptotic expansion. As such, the entire fluid domain is divided into two distinct regions: (1) the inner region encompassing the EDL with a characteristic length of δ and (2) the bulk or the outer region whose characteristic length scale remains $O(1)$. In either region any generic variable (say, ξ) may be asymptotically expanded in δ as follows:

$$\xi = \xi^{(0)} + \delta\xi^{(1)} + \cdots. \tag{5}$$

Subsequently, the inner and the outer layer variables have to be asymptotically matched at the edge of the EDL. In what follows, we shall consider only the leading order problem in δ, and hence the superscript "(0)" will not be used hereafter.

Inside the EDL (i.e., the inner layer), several of the variables will require rescaling, given that the relevant length scale there is δ. In particular, the shear strain rate within the EDL scales as $O(\delta^{-1})$, which coupled with the viscoelastic nature of the medium will result in the normal stresses ($\tau_{\theta\theta}$, $\tau_{\phi\phi}$, along with $\tau_{\theta\phi}$) scaling as $O(\delta^{-2})$ [7,8]. The remaining shear stress components scale

as $O(\delta^{-1})$. On the other hand, the θ and the ϕ components of the velocity remain $O(1)$, while the r-component scales as $O(\delta)$ [7]. The detailed rescaled equations within the EDL have been included in Appendix A 1; see Eqs. (A1). Subsequently, in Appendix A 2 we also invoke the weak charge approximation ($\bar{\zeta}_0 \ll 1$) in the inner layer equations and ignore all $O(\bar{\zeta}_0)$ and higher order terms appearing therein. Finally, the weak viscoelasticity approximation is enforced by expanding the relevant variables in both layers in an asymptotic series of De as follows:

$$\xi = \xi_0 + \mathrm{De}\xi_1 + \cdots . \tag{6}$$

Note that in Eq. (6), ξ represents leading order variables in δ. The detailed solutions to the leading order and the $O(\mathrm{De})$ velocity and pressure fields within the EDL have been included in Appendix A 2; see Eqs. (A3) and (A4). It is important to note that the particle's translational and the angular velocities ($\boldsymbol{\mathcal{U}}$ and $\boldsymbol{\Omega}$, respectively) also have expansions similar to Eq. (6).

In the leading order of δ, the flow in the inner layer drives the outer layer fluid through the Smoluchowski slip velocity ($\mathbf{V}_{HS}$), which is essentially the velocity at the edge of the EDL (or the inner layer) parallel to the particle surface. Therefore, one of the main purposes of solving the inner layer equations is to determine this slip velocity at the outer edge of the EDL, which may then be used to compute the flow in the bulk (i.e., the outer layer). In a viscoelastic medium, the Smoluchowski slip velocity gets modified, as discussed further below.

3. The modified Smoluchowski slip velocity $\mathbf{V}_{HS}$

Formally, the Smoluchowski slip velocity can be evaluated using the matching condition for the velocity at the edge of the EDL as follows:

$$\mathbf{V}_{HS} = \lim_{R\to\infty} [U\hat{\mathbf{e}}_{\bar{\theta}} + W\hat{\mathbf{e}}_{\bar{\phi}}] - \boldsymbol{\Omega}\times\hat{\mathbf{e}}_{\bar{r}}, \tag{7}$$

where R is the inner layer coordinate (see Appendix A), and U and W are respectively the $\bar{\theta}$ and the $\bar{\phi}$ components of the velocity in the inner layer. Akin to other variables, $\mathbf{V}_{HS}$ also has an asymptotic expansion in De, which reads

$$\mathbf{V}_{HS} = \mathbf{V}_{HS}^{(0)} + \mathrm{De}\mathbf{V}_{HS}^{(1)} + \cdots , \tag{8}$$

where $\mathbf{V}_{HS}^{(k)} = V_{HS,\bar{\theta}}^{(k)}\hat{\mathbf{e}}_{\bar{\theta}} + V_{HS,\bar{\phi}}^{(k)}\hat{\mathbf{e}}_{\bar{\phi}}$, $k = 0,\ 1, \ldots$. In Eq. (8), $\mathbf{V}_{HS}^{(0)}$ is the slip velocity in a Newtonian fluid, while the $O(\mathrm{De})$ correction accounts for the influence of viscoelasticity on the inner layer kinetics. Using the solutions for the velocity fields U and W as presented in Appendix A 2, the orderwise expressions of $\mathbf{V}_{HS}^{(k)}$ may be deduced as follows:

$$V_{HS,\bar{\theta}}^{(0)} = \frac{3}{2}\alpha\sqrt{1-\eta^2}\breve{\zeta}(\bar{\theta},\bar{\phi}), \quad V_{HS,\bar{\phi}}^{(0)} = 0, \tag{9a}$$

$$V_{HS,\bar{\theta}}^{(1)} = (1-\lambda_2)\Bigg[-\frac{9\eta\alpha^2}{2(1-\eta^2)^{3/2}}\omega_1^2 + \omega_1\Bigg(\frac{3\alpha\eta}{1-\eta^2}\Gamma_1 - \frac{27\alpha^2}{\sqrt{1-\eta^2}}\omega_{1,\eta} - \frac{3\alpha}{\sqrt{1-\eta^2}}\omega_2\Bigg) + 3\alpha\Gamma_1\omega_{1,\eta} - \frac{3\alpha}{1-\eta^2}\chi_1\omega_{1,\bar{\phi}}\Bigg], \tag{9b}$$

$$V_{HS,\bar{\phi}}^{(1)} = -(1-\lambda_2)\frac{3\alpha\omega_1\omega_3}{\sqrt{1-\eta^2}}. \tag{9c}$$

In the above, $\omega_1 = \breve{\zeta}(\bar{\theta},\bar{\phi})Q_1(\eta)$, $Q_1(\eta) = \frac{1}{2}(\eta^2-1)$ is the Gegenbauer polynomial [30] of order 1, $\Gamma_1 = \Omega_y^{(0)}\cos(\bar{\phi}) - \Omega_x^{(0)}\sin(\bar{\phi})$, $\omega_2 = \chi_{1,\bar{\phi}} + \eta\Gamma_1/\sqrt{1-\eta^2}$, where $\chi_1 = \Omega_z^{(0)}\sqrt{1-\eta^2} - \eta[\Omega_x^{(0)}\cos(\bar{\phi}) + \Omega_y^{(0)}\sin(\bar{\phi})]$ and $\omega_3 = \sqrt{1-\eta^2}\chi_{1,\bar{\phi}} + \frac{\eta\chi_1}{\sqrt{1-\eta^2}}$; further $\omega_{1,\eta} = \partial\omega_1/\partial\eta$, $\omega_{1,\bar{\phi}} = \partial\omega_1/\partial\bar{\phi}$, etc., whereas $\boldsymbol{\Omega}_k = \Omega_x^{(k)}\hat{\mathbf{e}}_x + \Omega_y^{(k)}\hat{\mathbf{e}}_y + \Omega_z^{(k)}\hat{\mathbf{e}}_z$.

There are several important features of the $O(\mathrm{De})$ slip velocity that are noteworthy. To begin, we observe that $\mathbf{V}_{HS}^{(1)}$ depends on the leading order angular velocity of the particle ($\boldsymbol{\Omega}_0$), which is of the form [as shown later in Eq. (31b)] $\mathcal{E}_1 + \alpha\mathcal{E}_2$ owing to the presence of an external flow. Therefore, the $O(\mathrm{De})$ slip velocity takes the form $\alpha\mathcal{G}_1(\bar{\theta}, \bar{\phi}) + \alpha^2\mathcal{G}_2(\bar{\theta}, \bar{\phi})$ [as evident from Eq. (9)] and hence will indirectly depend on the imposed flow through the leading order rotational velocity of the particle due to the linear terms in α (e.g., $\alpha\mathcal{G}_1$). This is in stark contrast to Newtonian fluids, where the Smoluchowski slip is independent of any external flow (provided that the flow is not too strong). It thus becomes evident that in a viscoelastic medium, the motion in the outer layer cannot be a linear superposition of the individual contributions from a pure shear flow and pure electrophoresis.

In the absence of any imposed shear flow, $\alpha \gg 1$ and hence $\alpha^2 \gg \alpha$. The $O(\mathrm{De})$ slip velocity in this limit may be derived by neglecting the $O(\alpha)$ terms in Eqs. (9b) and (9c), and it may then be shown that the resulting expressions are identical to those reported in Ref. [8]. Furthermore, the nonlinear relation between the modified slip velocity and the applied electric field as reported in earlier studies [7,8] is indeed preserved here. Finally, although there are no azimuthal components of the slip velocity in the leading order ($V_{HS,\bar{\phi}}^{(0)} = 0$), the ϕ component of $\mathbf{V}_{HS}^{(1)}$ turns out to be nonzero at $O(\mathrm{De})$; see Eq. (9c). Later we will establish that this will have important implications with regard to particle migration under the action of applied electric fields.

4. Simplified equations in the outer layer

Following the work of [60,61], it may be shown that in the outer region (bulk), the salt concentration, the net charge density and the EDL potential have the following solutions in the leading order of δ: $c = 2$, $\tilde{\rho} = 0$ (or equivalently $\rho = 0$), and $\varphi = 0$. Therefore in the thin EDL limit, the simplified outer layer equations governing the flow take the following form:

$$-\nabla p + \nabla \cdot \boldsymbol{\tau} = 0, \quad \text{and} \quad \nabla \cdot \mathbf{v} = 0. \tag{10a}$$

$$\boldsymbol{\tau} + \mathrm{De}\boldsymbol{\mathcal{T}} = 2\mathbf{D} + 2\lambda_2 \mathrm{De}\boldsymbol{\mathcal{S}}. \tag{10b}$$

They are subjected to the following boundary conditions, expressed w.r.t. the *central axis*:

$$\mathbf{v}(\bar{r} = 1, \bar{\theta}, \bar{\phi}) = \boldsymbol{\Omega} \times \hat{\mathbf{e}}_{\bar{r}} + \boldsymbol{\mathcal{U}} + \mathbf{V}_{HS}, \tag{11a}$$

$$\mathbf{v}(\bar{r} \to \infty, \bar{\theta}, \bar{\phi}) = \mathbf{v}_\infty = (\bar{y} + y_0)\hat{\mathbf{e}}_z. \tag{11b}$$

It is important to note that Eq. (11a) accounts for the Smoluchowski slip velocity ($\mathbf{V}_{HS}$) at the edge of the EDL, when imposing the boundary condition at the particle surface. Enforcing $\mathbf{V}_{HS}$ from Eq. (9), Eqs. (10) may be solved subject to the Eqs. (11), along with the force and torque balance conditions as mentioned in Eq. (3) to determine $\boldsymbol{\mathcal{U}}$ and $\boldsymbol{\Omega}$. These velocities may be subsequently used to track the particle's trajectory, as discussed below.

III. ASYMPTOTIC ANALYSIS FOR THE INSTANTANEOUS PARTICLE VELOCITIES

From our knowledge of $\mathbf{V}_{HS}$, we may evaluate the instantaneous linear and angular velocities of the particle using the outer layer equations (10) and the corresponding boundary conditions (11). To this end, it will be assumed that $\check{\zeta}(\bar{\theta}, \bar{\phi})$ is known on the particle surface at the given time instant but is otherwise arbitrary. The linear and the angular velocities of the particle may be expanded as

$$\boldsymbol{\mathcal{U}} = \boldsymbol{\mathcal{U}}_0 + \mathrm{De}\boldsymbol{\mathcal{U}}_1 + O(\mathrm{De}^2), \tag{12a}$$

$$\boldsymbol{\Omega} = \boldsymbol{\Omega}_0 + \mathrm{De}\boldsymbol{\Omega}_1 + O(\mathrm{De}^2), \tag{12b}$$

where $\boldsymbol{\mathcal{U}}_0$ and $\boldsymbol{\Omega}_0$ denote the particle velocities in a Newtonian medium and $\boldsymbol{\mathcal{U}}_1$ and $\boldsymbol{\Omega}_1$ quantify the first corrections due to the viscoelasticity of the medium. In what follows, we shall only evaluate the first two terms in the above asymptotic series, from which the particle trajectories will be subsequently determined. Furthermore, we will be using the *central axis* (see Sec. II A and Fig. 1) for evaluating the velocity field throughout this section.

A. The leading order solution

Enforcing the asymptotic expansion (6) in Eqs. (10), the leading order equations may be written as follows: $\boldsymbol{\tau}_0 = 2\boldsymbol{D}_0$, $-\boldsymbol{\nabla} p_0 + \nabla^2 \mathbf{v}_0 = 0$, and $\boldsymbol{\nabla} \cdot \mathbf{v}_0 = 0$, subject to $\mathbf{v}_0(\bar{r} = 1, \bar{\theta}, \bar{\phi}) = \boldsymbol{\Omega}_0 \times \hat{\mathbf{e}}_{\bar{r}} + \boldsymbol{\mathcal{U}}_0 + \mathbf{V}_{HS}^{(0)}$ and $\mathbf{v}_0(\bar{r} \to \infty, \bar{\theta}, \bar{\phi}) \to \mathbf{v}_\infty$, where the expression for $\mathbf{V}_{HS}^{(0)}$ is given in Eq. ((9) Recall that in order to evaluate the particle velocities, we need to impose the force and torque-free conditions [see Eq. (3)], which at the leading order take the form $\int_{S_p} (-p_0 \boldsymbol{I} + \boldsymbol{\tau}_0) \cdot \hat{\mathbf{e}}_{\bar{r}}\, dS = 0$ and $\int_{S_p} \hat{\mathbf{e}}_{\bar{r}} \times (\boldsymbol{\tau}_0 \cdot \hat{\mathbf{e}}_{\bar{r}})\, dS = 0$.

In an effort to systematically evaluate $\boldsymbol{\mathcal{U}}_0$, $\boldsymbol{\Omega}_0$, along with the leading order velocity field ($\mathbf{v}_0$), we use the Lamb's general solution by defining a disturbance velocity field to the externally imposed flow owing to the presence of the charged sphere as follows [50,62]: $\mathbf{v}_{0(d)} = \mathbf{v}_0 - \mathbf{v}_\infty$ (note that $\mathbf{v}_\infty$ and $\mathbf{v}_{0,\infty}$ are identical). The disturbance velocity field $\mathbf{v}_{0(d)}$ satisfies the same equations as $\mathbf{v}_0$, subject to $\mathbf{v}_{0(d)}(\bar{r} = 1, \bar{\theta}, \bar{\phi}) = \boldsymbol{\Omega}_0 \times \hat{\mathbf{e}}_{\bar{r}} + \boldsymbol{\mathcal{U}}_0 + \mathbf{V}_{HS}^{(0)} - \mathbf{v}_\infty(\bar{r} = 1, \bar{\theta}, \bar{\phi})$ and $\mathbf{v}_{0(d)}(\bar{r} \to \infty, \bar{\theta}, \bar{\phi}) \to 0$. We may use the Lamb's general solution [49] to evaluate $\mathbf{v}_{0(d)}$, which may be expressed terms of the solids harmonics $\Lambda_{-(n+1)}$, $\mathcal{Q}_{-(n+1)}$ and $\mathcal{P}_{-(n+1)}$, where $-(n+1)$ denotes their order. Using the *central axis*, we may therefore write

$$\mathbf{v}_{0(d)} = \sum_{n=1}^{\infty} \left[\boldsymbol{\nabla} \times (\bar{\mathbf{r}} \Lambda_{-(n+1)}) + \boldsymbol{\nabla} \mathcal{Q}_{-(n+1)} - \frac{n-2}{2n(2n-1)} \bar{r}^2 \boldsymbol{\nabla} \mathcal{P}_{-(n+1)} + \frac{n+1}{n(2n-1)} \bar{\mathbf{r}} \mathcal{P}_{-(n+1)} \right], \tag{13}$$

where $\bar{\mathbf{r}} = \bar{r}\hat{\mathbf{e}}_{\bar{r}}$. The solid harmonics $\mathcal{P}_{-(n+1)}$ has the following expression:

$$\mathcal{P}_{-(n+1)} = \bar{r}^{-n-1} \sum_{l=0}^{n} P_n^l(\eta)[A_{\ln} \cos(l\bar{\phi}) + \tilde{A}_{\ln} \sin(l\bar{\phi})], \tag{14}$$

while the expressions for the two remaining harmonics are also of the similar form and have been provided in Appendix B; see Eq. (B1). In the above, $P_n^l(\eta)$ is the associated Legendre polynomial of degree n and l. The unknown coefficients $A_{\ln}$, $\tilde{A}_{\ln}$, ..., etc., may be evaluated using the boundary condition for $\mathbf{v}_{0(d)}$ on the particle surface. The detailed procedure for evaluating the coefficients along with their expressions may be found in Refs. [8,63]. A brief outline of this method has also been included in Appendix B; see Eq. (B3).

Once the coefficients $A_{\ln}$, $\tilde{A}_{\ln}$, ..., etc., are known, we may impose the hydrodynamic force and torque free conditions, which may be recast using the solid harmonics as follows [49]:

$$\boldsymbol{\mathcal{F}} = -4\pi \boldsymbol{\nabla}(\bar{r}^3 \mathcal{P}_{-2}) = 0, \tag{15a}$$

$$\boldsymbol{T} = -8\pi \boldsymbol{\nabla}(\bar{r}^3 \Lambda_{-2}) = 0. \tag{15b}$$

From the above two conditions, the force balance yields $A_{01} = A_{11} = \tilde{A}_{11} = 0$, while the torque balance results in $C_{01} = C_{11} = \tilde{C}_{11} = 0$. Since these coefficients themselves contain the unknowns $\boldsymbol{\mathcal{U}}_0$ and $\boldsymbol{\Omega}_0$, equating them to zero will directly yield the leading order linear and angular particle velocities for a specific surface charge distribution $\breve{\zeta}(\bar{\theta}, \bar{\phi})$.

B. The viscoelastic [O(De)] corrections

1. The generalized reciprocal theorem

The equations governing the fluid flow at O(De) are rather complicated and not amenable to analytical solutions. However, since we are mainly interested in the linear and angular velocities of the particle, the calculations may be considerably simplified by making use of the generalized Reciprocal theorem [36,50]. As such, before proceeding, we shall first briefly state the theorem itself. Consider a (nondimensional) primary flow field ($\mathbf{v}$, p) around a spherical particle that satisfies the creeping flow equations as $\boldsymbol{\nabla} \cdot \boldsymbol{\Theta} + \mathbf{b} = 0$ and $\boldsymbol{\nabla} \cdot \mathbf{v} = 0$, where $\boldsymbol{\Theta} = -p\mathbf{I} + \boldsymbol{\tau}$ is the total stress tensor, $\boldsymbol{\tau} = 2\mathbf{D}$ is the deviatoric stress, and $\mathbf{b}$ is the body force per unit volume. Consider further an auxiliary flow field around that same particle ($\hat{\mathbf{v}}$, $\hat{p}$) with an analogously defined stress tensor ($\hat{\boldsymbol{\Theta}}$)

which satisfies $\nabla \cdot \hat{\boldsymbol{\Theta}} = 0$ and $\nabla \cdot \hat{\mathbf{v}} = 0$. Assuming that $\hat{\mathbf{v}}$ decays away from the particle and that the stresses in the primary flow field decay faster than $1/\bar{r}^2$, the generalized reciprocal theorem may be expressed as

$$\int_{S_p} \hat{\mathbf{e}}_{\bar{r}} \cdot \boldsymbol{\Theta} \cdot \hat{\mathbf{v}}\, dS - \int_{S_p} \hat{\mathbf{e}}_{\bar{r}} \cdot \hat{\boldsymbol{\Theta}} \cdot \mathbf{v}\, dS = \int_{\mathcal{V}} \mathbf{b} \cdot \hat{\mathbf{v}}\, d\mathcal{V}. \tag{16}$$

In the above, the integrations on the l.h.s. are carried out over the particle surface, and the one on the r.h.s. is over the entire fluid volume.

We shall first apply the reciprocal theorem to the leading order problem (which we have already solved using the Lamb's general solution) to have an alternative derivation as well as to test the theorem's validity. Recall that in the leading order, $\mathbf{b}_0 = 0$ and $\boldsymbol{\Theta}_{0(d)} = -p_0\mathbf{I} + 2\mathbf{D}_{0(d)}$, where $\boldsymbol{\Theta}_{0(d)} = \boldsymbol{\Theta}_0 - \boldsymbol{\Theta}_{0,\infty}$ is the perturbed stress field ($\boldsymbol{\Theta}_0$ and $\boldsymbol{\Theta}_{0,\infty}$ also have analogous definitions) and $\mathbf{D}_{0(d)}$ is the strain rate emanating from the disturbance velocity field $\mathbf{v}_{0(d)}$. Noting that $\boldsymbol{\Theta}_{0(d)}$ decays faster than $1/\bar{r}^2$, Eq. (16) may be simplified to

$$\int_{S_p} \hat{\mathbf{e}}_{\bar{r}} \cdot \boldsymbol{\Theta}_{0(d)} \cdot \hat{\mathbf{v}}\, dS = \int_{S_p} \hat{\mathbf{e}}_{\bar{r}} \cdot \hat{\boldsymbol{\Theta}} \cdot \mathbf{v}_{0(d)}\, dS. \tag{17}$$

In what follows, we shall use two types of auxiliary flow fields in order to evaluate the translational and angular velocities of the particle. These two are as follows:

(i) For evaluating $\boldsymbol{\mathcal{U}}$, we choose the flow field generated by a sphere translating with velocity $\hat{\mathbf{e}}$ (a unit vector pointing in any arbitrary direction) in a Newtonian fluid, as the auxiliary flow.

(ii) For evaluating $\boldsymbol{\Omega}$, we choose the flow field generated by a sphere rotating with angular velocity $\hat{\mathbf{e}}$ in a Newtonian fluid, as the auxiliary flow.

For auxiliary flow field (i), the traction on the particle's surface evaluates as [64] $\hat{\mathbf{e}}_{\bar{r}} \cdot \hat{\boldsymbol{\Theta}} = -\frac{3}{2}\hat{\mathbf{e}}$. At the same time, on S_p, $\mathbf{v}_{0(d)} = \boldsymbol{\mathcal{U}}_0 + \boldsymbol{\Omega}_0 \times \hat{\mathbf{e}}_{\bar{r}} + \mathbf{V}_{HS}^{(0)} - \mathbf{v}_\infty$ [from Eq. (11)], $\hat{\mathbf{v}} = \hat{\mathbf{e}}$, whereas the force-free condition simplifies to $\int_{S_p} \boldsymbol{\Theta}_0 \cdot \hat{\mathbf{e}}_{\bar{r}}\, dS = \int_{S_p} \boldsymbol{\Theta}_{0(d)} \cdot \hat{\mathbf{e}}_{\bar{r}}\, dS = 0$, since $\int_{S_p} \boldsymbol{\Theta}_{0,\infty} \cdot \hat{\mathbf{e}}_{\bar{r}}\, dS = 0$ identically. As a result, Eq. (17) may be further simplified to deduce the following expression for $\boldsymbol{\mathcal{U}}_0$:

$$\boldsymbol{\mathcal{U}}_0 = -\frac{1}{4\pi} \int_{Sp} \left(\mathbf{V}_{HS}^{(0)} - \mathbf{v}_\infty\right) dS, \tag{18}$$

which is of course a well-known result [62]. In Eq. (18) we have used the fact that $\mathbf{v}_{0,\infty} = \mathbf{v}_\infty$.

Similarly, for auxiliary field (ii), the traction on S_p evaluates as [64]: $\hat{\mathbf{e}}_{\bar{r}} \cdot \hat{\boldsymbol{\Theta}} = -3\hat{\mathbf{e}} \times \hat{\mathbf{e}}_{\bar{r}}$, while $\hat{\mathbf{v}} = \hat{\mathbf{e}} \times \hat{\mathbf{e}}_{\bar{r}}$. The torque free condition simplifies to $\int_{S_p} \hat{\mathbf{e}}_{\bar{r}} \times (\boldsymbol{\Theta}_{0(d)} \cdot \hat{\mathbf{e}}_{\bar{r}}) dS = -\int_{S_p} \hat{\mathbf{e}}_{\bar{r}} \times (\boldsymbol{\Theta}_{0,\infty} \cdot \hat{\mathbf{e}}_{\bar{r}})\, dS = 0$, since the components of $\boldsymbol{\Theta}_{0,\infty}$ are constants. Using these in Eq. (17), the expression for the particle's leading order rotational velocity ($\boldsymbol{\Omega}_0$) may be evaluated as

$$\boldsymbol{\Omega}_0 = -\frac{3}{8\pi} \int_{S_p} \hat{\mathbf{e}}_{\bar{r}} \times \left(\mathbf{V}_{HS}^{(0)} - \mathbf{v}_\infty\right) dS. \tag{19}$$

It may be verified that the above expressions simplify to those reported in Ref. [8] when $\mathbf{v}_\infty = 0$.

2. The O(De) corrections using the reciprocal theorem

We first note that the convected derivatives appearing in Eq. (10) have asymptotic expansions of the form $\boldsymbol{\mathcal{T}} = \mathrm{De}\boldsymbol{\mathcal{T}}_1 + \cdots$ and $\boldsymbol{\mathcal{S}} = \mathrm{De}\boldsymbol{\mathcal{S}}_1 + \cdots$, since in the leading order, all polymeric stresses vanish identically. The deviatoric stresses at $O(\mathrm{De})$ may be expressed as [from Eq. (10b)] $\boldsymbol{\tau}_1 = 2\mathbf{D}_1 + \boldsymbol{\tau}_1^{\mathrm{exc}}$, where $\boldsymbol{\tau}_1^{\mathrm{exc}} = 2(\lambda_2 - 1)\boldsymbol{\mathcal{S}}_1$ is the excess polymeric stresses at this order, and the expression for $\boldsymbol{\mathcal{S}}_1$ may be computed using the definition of the convected derivative provided after Eq. (1). We further note that at $O(\mathrm{De})$, $\mathbf{v}_1 = \mathbf{v}_{1(d)}$, since $\mathbf{v}_{1,\infty} = 0$. However, because of the viscoelastic nature of the fluid, $\boldsymbol{\mathcal{S}}_{1,\infty}$ (and thereby the excess far field polymeric stresses) is nonzero and may be expressed as: $\boldsymbol{\mathcal{S}}_{1,\infty} = \mathbf{v}_{0,\infty} \cdot \nabla \boldsymbol{D}_{0,\infty} - (\nabla \mathbf{v}_{0,\infty})^T \cdot \boldsymbol{D}_{0,\infty} - \boldsymbol{D}_{0,\infty} \cdot (\nabla \mathbf{v}_{0,\infty})$. Akin to

Sec. III B 1, we may thus define $\boldsymbol{\mathcal{S}}_{1(d)} = \boldsymbol{\mathcal{S}}_1 - \boldsymbol{\mathcal{S}}_{1,\infty}$, which captures the excess polymeric stresses caused by the disturbance flow in the leading order. It then becomes possible to split the excess polymeric stresses $\boldsymbol{\tau}_1^{\text{exc}}$ into the contributions from the far field and the leading order disturbance flow as $\boldsymbol{\tau}_1^{\text{exc}} = \boldsymbol{\tau}_{1(d)}^{\text{exc}} + \boldsymbol{\tau}_{1,\infty}^{\text{exc}}$, where $\boldsymbol{\tau}_{1(d)}^{\text{exc}} = 2(\lambda_2 - 1)\boldsymbol{\mathcal{S}}_{1(d)}$ and $\boldsymbol{\tau}_{1,\infty}^{\text{exc}} = 2(\lambda_2 - 1)\boldsymbol{\mathcal{S}}_{1,\infty}$. By denoting $\boldsymbol{\Theta}_1 = -p_1\mathbf{I} + 2\mathbf{D}_1$, the equation governing fluid flow at $O(\text{De})$ may be written as $\boldsymbol{\nabla}\cdot\boldsymbol{\Theta}_1 + \mathbf{b}_1 = 0$ and $\boldsymbol{\nabla}\cdot\mathbf{v}_1 = 0$, where $\mathbf{b}_1 = \boldsymbol{\nabla}\cdot\boldsymbol{\tau}_1^{\text{exc}}$. It straightforward to show that $\boldsymbol{\nabla}\cdot\boldsymbol{\tau}_{1,\infty}^{\text{exc}} = 0$, and therefore $\mathbf{b}_1$ simplifies to $\mathbf{b}_1 = \boldsymbol{\nabla}\cdot\boldsymbol{\tau}_{1(d)}^{\text{exc}} = 2(\lambda_2 - 1)\boldsymbol{\nabla}\cdot\boldsymbol{\mathcal{S}}_{1(d)}$. As such, the reciprocal theorem [Eq. (16)] at $O(\text{De})$ may be written as

$$\int_{S_p} \hat{\mathbf{e}}_{\bar{r}}\cdot\boldsymbol{\Theta}_1\cdot\hat{\mathbf{v}}\,dS - \int_{S_p}\hat{\mathbf{e}}_{\bar{r}}\cdot\hat{\boldsymbol{\Theta}}\cdot\mathbf{v}_1\,dS = \int_{\mathcal{V}}\boldsymbol{b}_1\cdot\hat{\mathbf{v}}\,d\mathcal{V}. \tag{20}$$

Recall from Eq. (11a) that on S_p, $\mathbf{v}_1 = \boldsymbol{\mathcal{U}}_1 + \boldsymbol{\Omega}_1\times\hat{\mathbf{e}}_{\bar{r}} + \mathbf{V}_{HS}^{(1)}$. On the other hand, the force balance at $O(\text{De})$ yields $\int_{S_p}(\boldsymbol{\Theta}_1 + \boldsymbol{\tau}_1^{\text{exc}})\cdot\hat{\mathbf{e}}_{\bar{r}}\,dS = 0$. Using the fact that $\boldsymbol{\tau}_1^{\text{exc}} = 2(\lambda_2 - 1)\boldsymbol{\mathcal{S}}_1$, the force-free condition may be further simplified to

$$\int_{S_p}\boldsymbol{\Theta}_1\cdot\hat{\mathbf{e}}_{\bar{r}}\,dS = -\int_{S_p}2(\lambda_2 - 1)\boldsymbol{\mathcal{S}}_1\cdot\hat{\mathbf{e}}_{\bar{r}}\,dS. \tag{21}$$

Now, in order to evaluate $\boldsymbol{\mathcal{U}}_1$ we appeal to auxiliary field (i) outlined in Sec. III B 1. Then, using Eq. (21), the boundary conditions for $\mathbf{v}_1$ on S_p, and noting that $\hat{\mathbf{v}} = \hat{\mathbf{e}}$ on the particle surface, the particle velocity at $O(\text{De})$ can be deduced from Eq. (20) as follows:

$$\boldsymbol{\mathcal{U}}_1\cdot\hat{\mathbf{e}} = -\frac{1}{4\pi}\hat{\mathbf{e}}\cdot\int_{S_p}\mathbf{V}_{HS}^{(1)}\,dS + \frac{1}{3\pi}(\lambda_2 - 1)\left(\hat{\mathbf{e}}\cdot\int_{S_p}\boldsymbol{\mathcal{S}}_1\cdot\hat{\mathbf{e}}_{\bar{r}}\,dS + \int_{\mathcal{V}}\hat{\mathbf{v}}\cdot(\boldsymbol{\nabla}\cdot\boldsymbol{\mathcal{S}}_{1(d)})\,d\mathcal{V}\right). \tag{22}$$

Using the Gauss divergence theorem and noting that $\boldsymbol{\mathcal{S}}_1 = \boldsymbol{\mathcal{S}}_{1(d)} + \boldsymbol{\mathcal{S}}_{1,\infty}$, where all the components of $\boldsymbol{\mathcal{S}}_{1,\infty}$ are constants, the above expression may be further simplified to

$$\boldsymbol{\mathcal{U}}_1\cdot\hat{\mathbf{e}} = -\frac{1}{4\pi}\hat{\mathbf{e}}\cdot\int_{S_p}\mathbf{V}_{HS}^{(1)}\,dS - \frac{1}{3\pi}(\lambda_2 - 1)\int_{\mathcal{V}}\boldsymbol{\mathcal{S}}_{1(d)} : \boldsymbol{\nabla}\hat{\mathbf{v}}\,d\mathcal{V}. \tag{23}$$

The velocity field of the auxiliary flow $\hat{\mathbf{v}}$ reads [8,64]

$$\hat{\mathbf{v}} = \frac{3\hat{\mathbf{e}}}{4\bar{r}}\left(1 + \frac{1}{3\bar{r}^2}\right) + \frac{3(\hat{\mathbf{e}}\cdot\bar{\mathbf{r}})\bar{\mathbf{r}}}{4\bar{r}^3}\left(1 - \frac{1}{\bar{r}^2}\right). \tag{24}$$

At this point it is important to underline the significance of the individual terms appearing in Eq. (23). The first term above evaluates the contribution from the surface average of the $O(\text{De})$ slip velocity to the particle's movement, and physically, it signifies the impact of the excess polymeric stresses inside the EDL. The second term accounts for the contributions from the excess polymeric stresses in the bulk region. Computation of this term requires a detailed knowledge of the leading order velocity field, which has been outlined in Sec. III A.

We now evaluate the viscoelastic corrections to the particle's angular velocity by following a similar procedure. The torque-free condition reads $\int_{S_p}\hat{\mathbf{e}}_{\bar{r}}\times\{(\boldsymbol{\Theta}_1 + \boldsymbol{\tau}_1^{\text{exc}})\cdot\hat{\mathbf{e}}_{\bar{r}}\}\,dS = 0$, which upon simplification yields

$$\int_{S_p}\hat{\mathbf{e}}_{\bar{r}}\times(\boldsymbol{\Theta}_1\cdot\hat{\mathbf{e}}_{\bar{r}})\,dS = -2\text{De}(\lambda_2 - 1)\int_{S_p}\hat{\mathbf{e}}_{\bar{r}}\times(\boldsymbol{\mathcal{S}}_1\cdot\hat{\mathbf{e}}_{\bar{r}})\,dS. \tag{25}$$

The velocity field of auxiliary flow (ii) in Sec. III B 1 has the following expression:

$$\hat{\mathbf{v}} = \boldsymbol{\nabla}\times\left(\frac{\hat{\mathbf{e}}\cdot\bar{\mathbf{r}}\bar{\mathbf{r}}}{\bar{r}^3}\right). \tag{26}$$

Using Eqs. (25) and (26), the boundary condition for $\mathbf{v}_1$ on the surface of the sphere, and noting that $\hat{\mathbf{v}} = \hat{\mathbf{e}}\times\hat{\mathbf{e}}_{\bar{r}}$ on S_p, the viscoelastic correction to the particle's angular velocity may be estimated

from Eq. (20) as

$$\boldsymbol{\Omega}_1 \cdot \hat{\mathbf{e}} = -\frac{3}{8\pi}\hat{\mathbf{e}} \cdot \int_{S_p} \left(\hat{\mathbf{e}}_{\bar{r}} \times \mathbf{V}_{HS}^{(1)}\right) dS + \frac{(\lambda_2 - 1)}{4\pi}\Bigg[\hat{\mathbf{e}} \cdot \int_{S_p} \hat{\mathbf{e}}_{\bar{r}} \times (\boldsymbol{\mathcal{S}}_{1(d)} \cdot \hat{\mathbf{e}}_{\bar{r}})\, dS + \int_{\mathcal{V}} \hat{\mathbf{v}} \cdot (\boldsymbol{\nabla} \cdot \boldsymbol{\mathcal{S}}_{1(d)})\, d\mathcal{V}\Bigg]. \tag{27}$$

In the above, we have used the fact that the components of $\boldsymbol{\mathcal{S}}_{1,\infty}$ are constants, and hence its contribution to the integral over the particle surface vanishes. Using the Gauss divergence theorem, Eq. (27) may be recast as

$$\boldsymbol{\Omega}_1 \cdot \hat{\mathbf{e}} = -\frac{3}{8\pi}\hat{\mathbf{e}} \cdot \int_{S_p} \left(\hat{\mathbf{e}}_{\bar{r}} \times \mathbf{V}_{HS}^{(1)}\right) dS - \frac{(\lambda_2 - 1)}{4\pi} \int_{\mathcal{V}} \boldsymbol{\mathcal{S}}_{1(d)} : \boldsymbol{\nabla}\hat{\mathbf{v}}\, d\mathcal{V}. \tag{28}$$

The various components of $\boldsymbol{\mathcal{U}}_1$ and $\boldsymbol{\Omega}_1$ may be computed from Eqs, (23) and (27) respectively by appropriately choosing $\hat{\mathbf{e}}$. Akin to Eq. (23), the combined contributions of the excess polymeric stresses originating from the EDL, and the bulk are also embedded in Eq. (27). It is important to note that the far-field polymeric stresses, captured by the term $\boldsymbol{\mathcal{S}}_{1,\infty}$, are constants only because the imposed flow is linear in nature, and hence they do not directly influence the particle's movement. However, for other kinds of flows (such as the Poiseuille flow), the contributions from these stresses to the particle's translational and rotational velocities may indeed be nonzero at $O(\mathrm{De})$.

Enforcing Eqs. (18) [or, equivalently, Eq. (15a)] and (23) into Eq. (12a), and Eqs. (19) [or, equivalently, Eq. (15b)] and (27) into Eq. (12b), the translational and the angular velocities of the particle upto $O(\mathrm{De})$ may be determined for a specified $\breve{\zeta}(\bar{\theta}, \bar{\phi})$ on its surface.

C. Analytical examples of instantaneous particle velocities

To derive analytical insights into the particle's movement, we shall consider a relatively simple instantaneous surface charge distribution [$\breve{\zeta}(\eta, \bar{\phi})$] and derive closed form expressions for $\boldsymbol{\mathcal{U}}$ and $\boldsymbol{\Omega}$. To this end, we note that any arbitrary surface charge may be decomposed using surface harmonics as follows:

$$\breve{\zeta}(\eta, \bar{\phi}) = \sum_{n=0}^{\infty} \mathcal{J}_n(\eta, \bar{\phi}), \quad \text{where} \quad \mathcal{J}_n(\eta, \bar{\phi}) = \sum_{l=0}^{n} P_n^l(\eta)[a_{\mathrm{ln}} \cos(l\bar{\phi}) + \tilde{a}_{\mathrm{ln}} \sin(l\bar{\phi})]. \tag{29}$$

$\mathcal{J}_n$ is the surface harmonic of order n. The simplest possible nonconstant and nonaxisymmetric $\breve{\zeta}(\eta, \bar{\phi})$ would then include only up to the first harmonic, which leads to

$$\breve{\zeta}(\eta, \bar{\phi}) = a_0 + a_{10}P_1^0(\eta) + P_1^1(\eta)(a_{11} \cos\bar{\phi} + \tilde{a}_{11} \sin\bar{\phi}), \tag{30}$$

where the coefficients $a_0, a_{10}, a_{11}, \tilde{a}_{11}$ are assumed to be $O(1)$. We proceed to calculate $\boldsymbol{\mathcal{U}}$ and $\boldsymbol{\Omega}$ by first considering this generic surface charge and then explore certain special cases by assigning specific values to the coefficients and the nondimensional parameter α.

With the form of $\breve{\zeta}(\eta, \bar{\phi})$ mentioned as above, we evaluate the coefficients in the Lamb's general solution using the procedure outlined Appendix B. Subsequently, using the force and the torque-free

conditions from Eq. (15), the leading order particle velocities appear as

$$\boldsymbol{\mathcal{U}}_0 = (y_0 + a_0\alpha)\hat{\mathbf{e}}_z, \tag{31a}$$

$$\boldsymbol{\Omega}_0 = \left(\frac{3\tilde{a}_{11}\alpha}{4} + \frac{1}{2}\right)\hat{\mathbf{e}}_x + \left(\frac{-3a_{11}\alpha}{4}\right)\hat{\mathbf{e}}_y, \tag{31b}$$

where y_0 is the offset distance of the particle w.r.t. the laboratory-fixed axis. We would like to clarify that Eq. (31) expresses the particle velocities w.r.t. the *lab-fixed* as well as the *central axis*. It is evident from Eq. (31) that the total velocity (both translational and rotational) of the particle is simply a linear superposition of the electrophoretic contribution [the $O(\alpha)$ terms] and the external flow's contribution, as is expected in case of Newtonian fluids. It may be easily verified from Eqs. (18) and (19) that the reciprocal theorem also leads to identical results.

The leading order velocity field $\mathbf{v}_0$ may be deduced by using the procedure described in Appendix B, although we do not report it here for the sake of brevity. We may subsequently use Eqs. (23) and (27) to determine the $O(\mathrm{De})$ corrections to the particle velocities as follows:

$$\begin{aligned}\boldsymbol{\mathcal{U}}_1 = (1-\lambda_2)\big[&-\tfrac{39}{20}\big(\alpha^2 a_0 a_{11} - \tfrac{1}{26}\alpha^2 a_{10}\tilde{a}_{11} - \tfrac{1}{39}\alpha a_{10}\big)\hat{\mathbf{e}}_x - \tfrac{39}{20}\alpha^2\big(a_0\tilde{a}_{11} + \tfrac{1}{26}a_{10}a_{11}\big)\hat{\mathbf{e}}_y \\ &- \alpha^2\big(\tfrac{3}{5}a_0 a_{10}\big)\hat{\mathbf{e}}_z\big],\end{aligned} \tag{32a}$$

$$\begin{aligned}\boldsymbol{\Omega}_1 = (1-\lambda_2)\big\{&\big[\tfrac{9}{80}\alpha^2(a_0 a_{11} + 5a_{10}\tilde{a}_{11}) + \tfrac{22}{3}a_{10}\alpha\big]\hat{\mathbf{e}}_x + \tfrac{3}{80}(3a_0\tilde{a}_{11}\alpha^2 - 15a_{10}a_{11}\alpha^2 + 2a_0\alpha)\hat{\mathbf{e}}_y \\ &- \tfrac{3}{10}\alpha a_{11}\hat{\mathbf{e}}_z\big\}.\end{aligned} \tag{32b}$$

The instantaneous particle velocities with respect to the laboratory-fixed axis (or, the central axis) up to $O(\mathrm{De})$ may therefore be computed using Eq. (12).

There are several key points to be noted from the $O(\mathrm{De})$ particle velocities. First, we observe that both $\boldsymbol{\mathcal{U}}_1$ and $\boldsymbol{\Omega}_1$ have the form, $\mathcal{C}_1\alpha + \mathcal{C}_2\alpha^2$, where the terms proportional to α^2 result from pure electrophoretic motion, and the terms proportional to α indicate motion originating from the nonlinear interactions between electrophoresis and the externally imposed flow. Second, the $O(\mathrm{De})$ velocity has components along all three directions, thus indicating that the particle will tend to migrate along the x and y directions, while the z component of the velocity also has corrections at $O(\mathrm{De})$. If $\alpha = 0$, $\boldsymbol{\mathcal{U}}_1 = \boldsymbol{\Omega}_1 = 0$, which implies that the presence of an electric field is necessary for particle migration to take place, although both electrophoresis and the external flow eventually contribute to it. Third, we note from Eq. (32b) that $\Omega_z^{(1)} \propto \alpha$, which again indicates that the rotation around the z axis comes about because of the nonlinear interactions between the electrophoretic motion and the background flow and is otherwise absent if either of these two agents vanish. Fourth, the offset distance y_0 only seems to influence the leading order velocity. This is of course expected, since any offset distance along the y axis is simply equivalent to adapting a different inertial frame moving with the offset velocity and thus should not result in any corrections at $O(\mathrm{De})$.

1. Special case I: Axisymmetric surface charge (a_0, $a_{10} \neq 0$; a_{11}, $\tilde{a}_{11} = 0$)

For this special case, the charge distribution takes the form $\breve{\zeta}(\theta) = a_0 + a_{10}\eta$. Therefore, from Eqs. (31) and (32), the particle velocities are evaluated as: $\boldsymbol{\mathcal{U}} = (y_0 + a_0\alpha)\hat{\mathbf{e}}_z + \mathrm{De}(1-\lambda_2)[(1/20)\alpha a_{10}\hat{\mathbf{e}}_x - (3/5)\alpha^2 a_0 a_{10}\hat{\mathbf{e}}_z]$ and $\boldsymbol{\Omega} = (1/2)\hat{\mathbf{e}}_x + \mathrm{De}(1-\lambda_2)[(22/3)\alpha a_{10}\hat{\mathbf{e}}_x + (3/40)\alpha a_0\hat{\mathbf{e}}_y]$. Remarkably, even though the surface charge distribution is axisymmteric, we still witness a migratory velocity along the x direction at $O(\mathrm{De})$. It has been shown by Borthakur and Ghosh [8] [see also Eq. (33a)] that pure electrophoretic motion of axisymmetrically charged particles does not result in any migration perpendicular to the direction of the applied electric field. Similarly, a particle in a pure shear flow ($\alpha = 0$) will also not exhibit any lateral migration. Therefore, we conclude that the nonzero $\mathcal{U}_{1,x}$ [which is $O(\alpha)$] reported above must be borne out of the nonlinear interactions between the externally imposed flow and the electrophoretic movement of the particle.

2. Special case II: Pure shear ($\alpha = 0$)

In the absence of any electrophoretic motion, $\alpha = 0$, and the resulting particle velocities become $\boldsymbol{\mathcal{U}} = y_0\hat{\mathbf{e}}_z$ and $\boldsymbol{\Omega} = (1/2)\hat{\mathbf{e}}_x$. Therefore, the particle simply rotates with a constant angular velocity and moves in a straight line, while the viscoelastic nature of the surrounding medium has no influence on its motion, at least up to $O(\mathrm{De})$. This is simply because the problem becomes inherently symmetric when $\alpha = 0$, and thus the polymeric stress arising at $O(\mathrm{De})$ does not contribute to either particle's translation and rotation. The presence of an electric field, however, breaks this fore-aft symmetry, and this phenomenon does not seem to occur in a Newtonian medium in the creeping flow limit.

3. Comparison with the existing literature

Several special cases of the analytical results reported here may be compared with the existing literature. First, the expression for the $O(\mathrm{De})$ correction to the particle's translational as expressed in Eq. (23) is very similar to the one reported by Li and Koch [36], who considered pure electrophoretic motion of a uniformly charged particle, although in their study, the first correction came at $O(\mathrm{De}^2)$. Second, in a Newtonian medium ($\mathrm{De} = 0$), for pure electrophoretic motion of a particle carrying a surface charge as given in Eq. (30), its translational and rotational velocities are given by [see Eq. (31)] $\boldsymbol{\mathcal{U}}_0 = \alpha a_0\hat{\mathbf{e}}_z$ and $\boldsymbol{\Omega}_0 = (3/4)\alpha(\tilde{a}_{11}\hat{\mathbf{e}}_x - a_{11}\hat{\mathbf{e}}_y)$. Anderson [2] derived general expressions for the electrophoretic velocities of nonuniformly charged spherical particles in a Newtonian fluid in the thin EDL limit, and it may be verified that the above expressions for the particular choice of $\breve{\zeta}$ match those reported by Anderson; also see the discussion ahead in Sec. V A 1.

For the viscoelastic corrections, the limit of pure electrophoretic motion may be recovered by enforcing $\alpha \gg 1$, which also mandates $\alpha^2 \gg \alpha$. As such, neglecting the $O(\alpha)$ terms in Eq. (32), we deduce

$$\boldsymbol{\mathcal{U}}_1 = \alpha^2(1-\lambda_2)\big[-\tfrac{39}{20}\big(a_0a_{11} - \tfrac{1}{26}a_{10}\tilde{a}_{11}\big)\hat{\mathbf{e}}_x - \tfrac{39}{20}\big(a_0\tilde{a}_{11} + \tfrac{1}{26}a_{10}a_{11}\big)\hat{\mathbf{e}}_y - \tfrac{3}{5}a_0a_{10}\hat{\mathbf{e}}_z\big], \quad (33a)$$

$$\boldsymbol{\Omega}_1 = \alpha^2(1-\lambda_2)\big\{\big[\tfrac{9}{80}(a_0a_{11} + 5a_{10}\tilde{a}_{11})\big]\hat{\mathbf{e}}_x + \big[\tfrac{3}{80}(3a_0\tilde{a}_{11} - 15a_{10}a_{11})\hat{\mathbf{e}}_y\big]\big\}, \quad (33b)$$

both of which agree with the velocity reported in Ref. [8]. Considering the special case of a particle carrying axisymmetric surface charge ($a_0,\ a_{10} \neq 0$ and $a_{11} = \tilde{a}_{11} = 0$), the electrophoretic velocity (pure electrophoresis) comes out to be $\boldsymbol{\mathcal{U}} = \alpha a_0\hat{\mathbf{e}}_z - (3/5)\mathrm{De}\alpha^2(1-\lambda_2)a_0a_{10}\hat{\mathbf{e}}_z$, which matches exactly that derived by Ghosh *et al.* [7]. Ghosh *et al.* [7] in turn validated their results for the special case of uniformly charged particles with Li and Koch [36].

It is evident from Eq. (32) that for a uniformly charged particle ($a_{10} = a_{11} = \tilde{a}_{11} = 0$), $\boldsymbol{\mathcal{U}}_1 = \mathbf{0}$, and hence the particle does not migrate, even in a viscoelastic medium. However, if one ignores the contributions from the $O(\mathrm{De})$ slip velocities to the particle's translational velocity; i.e., if the term $-\frac{1}{4\pi}\hat{\mathbf{e}}\cdot\int_{S_p}\mathbf{V}^{(1)}_{HS}\,dS$ in Eq. (23) is discarded, the resulting velocity at $O(\mathrm{De})$ becomes $\boldsymbol{\mathcal{U}}_1\cdot\hat{\mathbf{e}} = -(1/3\pi)(\lambda_2-1)\int_{\mathcal{V}}\boldsymbol{\mathcal{S}}_{1(d)} : \boldsymbol{\nabla}\hat{\mathbf{v}}\,d\mathcal{V}$. When evaluated for a uniformly charged particle (choosing $a_0 = 1$), this yields $\boldsymbol{\mathcal{U}}_1 = -\mathrm{De}\alpha(1-\lambda_2)/4\ \hat{\mathbf{e}}_y$ and shows a nonzero migration velocity in the y direction, as also reported by Khair and Kabarowski [46] [they also ignored the contributions from the $O(\mathrm{De})$ Smoluchowski slip velocity]. Using the appropriate characteristic scales mentioned earlier, the dimensional (with units) version of the above velocity becomes $\boldsymbol{\mathcal{U}}'_1 = -0.25G'(\lambda'_1 - \lambda'_2)u_E\hat{\mathbf{e}}_y = (-1/8)G'\mu^{-1}u_E\Lambda_1\hat{\mathbf{e}}_y$ or, $|\boldsymbol{\mathcal{U}}'_1| \sim \mu^{-1}\Lambda_1u_E$, where $\Lambda_1 = 2\mu(\lambda'_1 - \lambda'_2)$ is the first normal stress coefficient of an Oldroyd-B fluid [48]. Apart from the numeric prefactor, the above expression for the migration velocity agrees well with Khair and Kabarowski [46]'s result upon equating the second normal stress coefficient in their work to zero. Later Choudhary *et al.* [47] suggested a correction to their results for the migration velocity, and our result for $\boldsymbol{\mathcal{U}}'_1$ mentioned as above matches exactly that of Choudhary *et al.* [47] when the second normal stress coefficient is equated to zero. It is also worth noting that Khair and Kabarowski carried out their analysis for a second-order fluid, which has subtle differences with the Oldroyd-B model when $\mathrm{De} \ll 1$.

IV. CONSTRUCTING THE PARTICLE TRAJECTORIES

A. Equations governing the particle trajectories

Here we shall outline a general framework to construct the pathway followed by a particle under the following conditions: (1) the initial charge distribution of its surface, denoted as $\breve{\zeta}(\eta, \bar{\phi}; t = 0)$ (recall that $\eta = \cos\bar{\theta}$) is known and (2) the particle starts its journey from a given initial position, say, $\mathbf{x}_P(t = 0) = y_0\hat{\mathbf{e}}_y$, when measured using the *lab-fixed axis*. For obvious reasons, the particle trajectory will be computed only in the *lab-fixed axis*. The surface charge distribution at any instant $\breve{\zeta}(\eta, \bar{\phi}; t)$ will dictate the instantaneous translational and angular velocities of the particle. The translational velocity in turn will govern how the particle moves in space, and the angular velocity will dictate how the surface charge $\breve{\zeta}(\eta, \bar{\phi}; t)$ evolves in time in the central axis. This is precisely why $\breve{\zeta}$ also becomes a function of time when viewed in w.r.t. the central axis. In the same spirit, we shall denote the instantaneous velocities of the particle as $\boldsymbol{\mathcal{U}}[\breve{\zeta}(\eta, \bar{\phi}; t)]$ and $\boldsymbol{\Omega}[\breve{\zeta}(\eta, \bar{\phi}; t)]$, which stems from the fact that both $\boldsymbol{\mathcal{U}}$ and $\boldsymbol{\Omega}$ depend on the instantaneous distribution of $\breve{\zeta}$ (because of the quasisteady approximation) and may be computed using the analysis of Sec. III.

The position of the particle in the laboratory-fixed axis $[\mathbf{x}(t)]$ is related to its instantaneous velocity as

$$\frac{d\mathbf{x}_P}{dt} = \boldsymbol{\mathcal{U}}[\breve{\zeta}(\eta, \bar{\phi}; t)] = \boldsymbol{\mathcal{U}}_0[\breve{\zeta}(\eta, \bar{\phi}; t)] + \mathrm{De}\,\boldsymbol{\mathcal{U}}_1[\breve{\zeta}(\eta, \bar{\phi}; t)] + O(\mathrm{De}^2), \tag{34}$$

subject to $\mathbf{x}_P(0) = y_0\hat{\mathbf{e}}_y$. Further, since $\bar{\mathbf{x}} = \mathbf{x} - \mathbf{x}_P(t)$, it follows that the offset along the y axis plays a key role in governing the particle's velocity along the z direction, and as such for applying Eq. (34), y_0 should be replaced by $y_p(t)$ while evaluating $\mathbf{v}_0$ and thereby $\boldsymbol{\mathcal{U}}_0$ in Sec. III A.

We require an additional set of equations which are to be solved simultaneously along with Eq. (34) to specify $\breve{\zeta}(\eta, \bar{\phi}; t)$ on the particle surface. For this, we appeal to the *body-fixed axis* ($\tilde{r}'$, $\tilde{\theta}$, $\tilde{\phi}$ or, $\tilde{x}'$, $\tilde{y}'$, $\tilde{z}'$), which translates as well as rotates with the particle, and hence $\breve{\zeta}(\tilde{\theta}, \tilde{\phi}) = \breve{\zeta}(\eta, \bar{\phi}; t = 0)$ remains invariant with time w.r.t. this axis. Let $\hat{\boldsymbol{i}}(t)$, $\hat{\boldsymbol{j}}(t)$, and $\hat{\boldsymbol{k}}(t)$ be the unit vectors in the body-fixed axis, all of which are functions of time when evaluated w.r.t. the central (or the laboratory-fixed) axis, due to the particle's rotation. By tracking any two of these unit vectors, the orientation of the body-fixed axis w.r.t. the central axis will be known from which the instantaneous $\breve{\zeta}(\eta, \bar{\phi}, t)$ may be determined. The said unit vectors evolve as [8,65]

$$\frac{d\hat{\boldsymbol{j}}}{dt} = \boldsymbol{\Omega}[\breve{\zeta}(\eta, \bar{\phi}; t)] \times \hat{\boldsymbol{j}}, \quad \frac{d\hat{\boldsymbol{k}}}{dt} = \boldsymbol{\Omega}[\breve{\zeta}(\eta, \bar{\phi}; t)] \times \hat{\boldsymbol{k}}, \text{ and } \hat{\boldsymbol{i}} = \hat{\boldsymbol{j}}(t) \times \hat{\boldsymbol{k}}(t), \tag{35}$$

subject to $\hat{\boldsymbol{i}}(0) = \hat{\mathbf{e}}_x$, $\hat{\boldsymbol{j}}(0) = \hat{\mathbf{e}}_y$, and $\hat{\boldsymbol{k}}(0) = \hat{\mathbf{e}}_z$. Equations (34) and (35) may be integrated using the Euler explicit scheme to track the particle's pathway and the evolution of the body-fixed unit vectors. Recalling that $\breve{\zeta}(\tilde{\eta}, \tilde{\phi})$ (with $\tilde{\eta} = \cos\tilde{\theta}$) is invariant in time (and thus always remains identical to the initial distribution of $\breve{\zeta}$), we may determine $\breve{\zeta}(\eta, \bar{\phi}; t)$ by simply evaluating the $(\tilde{\eta}, \tilde{\phi})$ coordinates of a point on the particle surface from its $(\eta, \bar{\phi})$ coordinates. The relationship between $(\tilde{\eta},\ \tilde{\phi})$ and $(\eta,\ \bar{\phi})$ may be evaluated as follows [8]:

$$\tilde{\eta} = \eta\hat{k}_z(t) + \sqrt{1-\eta^2}\sin\bar{\phi}\ \hat{k}_y(t) + \sqrt{1-\eta^2}\cos\bar{\phi}\hat{k}_x(t), \tag{36a}$$

$$\sin\tilde{\phi} = \frac{\eta}{\sqrt{1-\tilde{\eta}^2}}\hat{j}_z(t) + \sqrt{\frac{1-\eta^2}{1-\tilde{\eta}^2}}\sin\bar{\phi}\ \hat{j}_y(t) + \sqrt{\frac{1-\eta^2}{1-\tilde{\eta}^2}}\cos\bar{\phi}\ \hat{j}_x(t), \tag{36b}$$

$$\cos\tilde{\phi} = \frac{\eta}{\sqrt{1-\tilde{\eta}^2}}\hat{i}_z(t) + \sqrt{\frac{1-\eta^2}{1-\tilde{\eta}^2}}\sin\bar{\phi}\ \hat{i}_y(t) + \sqrt{\frac{1-\eta^2}{1-\tilde{\eta}^2}}\cos\bar{\phi}\ \hat{i}_x(t). \tag{36c}$$

Here $\hat{i}_x,\ \hat{i}_y,\ \hat{i}_z, \ldots$, etc., are respectively the x, y, and z components of the body-fixed unit vectors $\hat{\boldsymbol{i}}$, $\hat{\boldsymbol{j}}$, and $\hat{\boldsymbol{k}}$.

To summarize, at any given time instant, we first compute the particle velocities using Eqs. (12) along with Eqs. (18), (23), (19), and (27) and plug them into (34) and (35) to deduce the particle's position and orientation at the next time instant. We then use Eqs. (36) and $\breve{\zeta}(\eta, \bar{\phi}; t = 0)$ to evaluate the surface charge distribution in the central axis at the next time step. The steps outlined above are repeated at every time step to construct the particle's trajectory. Finally, recall that computation of the $O(\mathrm{De})$ corrections to the particle velocity requires the leading order velocity field, which is of the form (13).

B. Numerical computation of the particle trajectories

We place an $\eta \times \bar{\phi}$ grid ($\eta \in [-1, 1]$, $\bar{\phi} \in [0, 2\pi]$) consisting of 150×300 elements, on which $\breve{\zeta}(\eta, \bar{\phi}; t)$ will be defined at any given time step. The leading order velocity field ($\mathbf{v}_0$) is subsequently computed using the Lamb's general solution and the boundary conditions on the particle's surface as outlined in Sec. III A and Appendix B on a 3D $\eta \times \bar{\phi} \times \bar{r}$ grid ($1 \leqslant \bar{r} \leqslant 20$) with $150 \times 300 \times 200$ grid points. The stresses ($\boldsymbol{\tau}_1$) and the convected derivative ($\boldsymbol{\mathcal{S}}_1$) are also computed on this same 3D grid. The grid along $\bar{r}$ is finer close to the particle to accurately capture the variations in the velocity. We have verified that changing the number of grid points does not change our results.

For integrating Eqs. (34) and (35), we use a time step size $\Delta t = 0.01$. We have ensured that this is sufficient to yield accurate results; see Appendix C for further details. Although in our framework any arbitrary number of modes may be taken to represent the surface charge distribution, in what follows we have considered up to $N = 7$ modes of solid harmonics, which includes a total of 35 modes of the associated Legendre polynomials, in an effort to limit the computational time. While computing the particle velocities, all integrations have been carried out using the trapezoidal rule.

V. RESULTS AND DISCUSSION

This section is arranged as follows. First, we shall explore particle dynamics in Newtonian medium (Sec. V A) and show that the trajectories may be constructed by solving a set of ordinary differential equations (what we refer to as the "Reduced Order Model") without detailed knowledge of the velocity field. In Sec. V B we shall discuss a few representative examples of particle trajectories in viscoelastic media, for specific choices of surface charge distributions. It will be shown that although the reduced order model discussed in Sec. V A does not directly apply to viscoelastic fluids, the insights derived from it will nevertheless be helpful in understanding particle motion therein.

A. Particle motion in Newtonian fluids

1. Reduced order equations for the particle trajectories

We shall derive ordinary differential equations governing the trajectory (and the velocity) of a particle in a Newtonian medium, subject to the specific circumstances being considered in this article. To this end we follow the lead of Anderson [2] and note that the electrophoretic component of the particle's velocities in a Newtonian fluid (denoted as, $\boldsymbol{\mathcal{U}}_0^E$ and $\boldsymbol{\Omega}_0^E$) may be represented using the multipole moments of its surface charge distribution. For instance, in the example considered in Eqs. (31), the electrophoretic components are $\boldsymbol{\mathcal{U}}_0^E = \alpha a_0 \hat{\mathbf{e}}_z$ and $\boldsymbol{\Omega}_0^E = (3\alpha/4)(\tilde{a}_{11}\hat{\mathbf{e}}_x - a_{11}\hat{\mathbf{e}}_y)$.The multipole moments are defined as follows (using the central axis):

$$\text{Monopole Moment:} \quad H^{(0)} = \langle \breve{\zeta}(\eta, \bar{\phi}) \rangle, \tag{37a}$$

$$\text{Dipole Moment:} \quad \mathbf{H}^{(1)} = \langle \breve{\zeta}(\eta, \bar{\phi}) \hat{\mathbf{e}}_{\bar{r}} \rangle, \tag{37b}$$

$$\text{Quadrupole Moment:} \quad \mathbf{H}^{(2)} = \langle \breve{\zeta}(\eta, \bar{\phi}) (3\hat{\mathbf{e}}_{\bar{r}}\hat{\mathbf{e}}_{\bar{r}} - \mathbf{I}) \rangle, \tag{37c}$$

where $\langle \cdot \rangle$ denotes the surface average and the superscript denotes the order of the moment. Anderson [2] showed that $\boldsymbol{\mathcal{U}}_0^E$ and $\boldsymbol{\Omega}_0^E$ are related to the multipole moments defined above, through the

following equations:

$$\boldsymbol{\mathcal{U}}_0^E = \mathcal{L}_0\big(H^{(0)}\mathbf{I} - \tfrac{1}{2}\mathbf{H}^{(2)}\big)\cdot\mathbf{E}_\infty \quad \text{and} \quad \boldsymbol{\Omega}_0^E = \mathcal{K}_0(\mathbf{H}^{(1)}\times\mathbf{E}_\infty), \tag{38}$$

where $\mathbf{E}_\infty = \hat{\mathbf{e}}_z$ is the imposed electric field away from the particle, $\mathcal{L}_0 = \alpha$ and $\mathcal{K}_0 = (9/4)\alpha$. It may be easily verified that the expressions in Eqs. (31) agree with the form given above.

The particle trajectories may be constructed by following the same procedure as outlined in Sec. IV A. To this end, we require the particle's orientation at any time, from which its instantaneous velocities may be computed, out of which the angular velocity will dictate how the orientation changes thereafter. However, examining Eq. (38), we realize that one does not need to know the detailed distribution of $\breve{\zeta}$ at every time instant; rather only the knowledge of the dipole and the quadrupole moments (the monopole moment is the net charge which is independent of the particle's orientation) are sufficient to uniquely determine the particle's instantaneous velocities. Moving ahead, we shall first outline the set of ODEs that govern the orientation as well as the multipole moments of the particle, following which the equations for its trajectories will be laid out.

Without the loss of generality we may choose $\hat{\boldsymbol{k}}$ to be oriented along the dipole moment $\mathbf{H}^{(1)}$ of the surface charge distribution, such that $\mathbf{H}^{(1)}(t) = H^{(1)}\hat{\boldsymbol{k}}(t)$ at all times, where $H^{(1)} = |\mathbf{H}^{(1)}| = \sqrt{(H_x^{(1)})^2 + (H_y^{(1)})^2 + (H_z^{(1)})^2}$, where $H_x^{(1)}(t) = \frac{1}{4\pi}\int_{S_p}\breve{\zeta}(\eta,\bar{\phi};t)\sqrt{1-\eta^2}\cos\bar{\phi}\,dS$ and so on. We would like to emphasize that $H^{(1)}$ is an invariant, since it denotes the magnitude of the dipole moment. The unit vector $\hat{\boldsymbol{j}}$ may be chosen along any convenient direction on the plane perpendicular to $\hat{\boldsymbol{k}}$, while $\hat{\boldsymbol{i}} = \hat{\boldsymbol{j}}\times\hat{\boldsymbol{k}}$, and this uniquely determines the orientation of the particle as well as the body-fixed axis. Note that we need to specify two unit vectors attached to the particle to uniquely prescribe its orientation because in general it may carry a nonaxisymmetric surface charge. Equation (35) governs the evolution of these unit vectors, wherein the angular velocity now becomes (Newtonian medium): $\boldsymbol{\Omega} = \boldsymbol{\Omega}_0 = \boldsymbol{\Omega}_0^E + \boldsymbol{\Omega}_0^\infty$, where $\boldsymbol{\Omega}_0^E$ is given by Eq. (38) and $\boldsymbol{\Omega}_0^\infty = \frac{1}{2}\hat{\mathbf{e}}_x$ is the rotation induced by the externally imposed flow (also see Sec. III C 2). Therefore, $\hat{\boldsymbol{k}}(t)$ and $\hat{\boldsymbol{j}}(t)$ are respectively governed by the equations

$$\frac{d\hat{\boldsymbol{k}}}{dt} = \frac{1}{2}\hat{\mathbf{e}}_x\times\hat{\boldsymbol{k}} + \mathcal{R}_0(\hat{\boldsymbol{k}}\times\hat{\mathbf{e}}_z)\times\hat{\boldsymbol{k}}, \tag{39a}$$

$$\frac{d\hat{\boldsymbol{j}}}{dt} = \frac{1}{2}\hat{\mathbf{e}}_x\times\hat{\boldsymbol{j}} + \mathcal{R}_0(\hat{\boldsymbol{k}}\times\hat{\mathbf{e}}_z)\times\hat{\boldsymbol{j}}, \tag{39b}$$

where $\mathcal{R}_0 = \frac{9}{4}\alpha H^{(1)}$, and we have used the fact that $\mathbf{H}^{(1)}(t) = H^{(1)}\hat{\boldsymbol{k}}(t)$ and $\mathbf{E}_\infty = \hat{\mathbf{e}}_z$. Equation (39a) is subject to $\hat{\boldsymbol{k}}(t=0) = \mathbf{H}^{(1)}(0)/H^{(1)}$, while the initial condition for $\hat{\boldsymbol{j}}$ depends on the choice of its orientation and can be arbitrary (subject to $\hat{\boldsymbol{j}}\cdot\hat{\boldsymbol{k}} = 0$). We would like to clarify here that unlike Fig. 1, the body-fixed and the central axis may not coincide at $t = 0$ in the present scenario. Further note that $\mathbf{H}^{(1)}(0)$ will be known from $\breve{\zeta}(\eta,\bar{\phi};t=0)$. The instantaneous angular velocity of the particle may then be evaluated as

$$\boldsymbol{\Omega}_0 = \big(\tfrac{1}{2} + \mathcal{R}_0\hat{k}_y\big)\hat{\mathbf{e}}_x - \mathcal{R}_0\hat{k}_x\hat{\mathbf{e}}_y. \tag{40}$$

Equations (39) offers a multitude of insights into the rotational motion of the particle, which in turn will govern its translation. First, observe that Eq. (39a) is nonlinear in $\hat{\boldsymbol{k}}$ whenever $\mathcal{R}_0 \neq 0$–a condition that is satisfied for nonuniform distributions of surface charge (because then $H^{(1)} > 0$). Therefore, one concludes that even in Newtonian fluids, externally imposed flow and electrophoresis can not be superimposed linearly when assessing the trajectories of nonuniformly charged particles. However, for a uniformly charged particle, $H^{(1)} = H_{mn}^{(2)} = 0$ (where $H_{mn}^{(2)}$ is the mnth component of the quadrupole moment in the central axis) identically, and hence Eq. (39a) simplifies to $d\hat{\boldsymbol{k}}/dt = (1/2)\hat{\mathbf{e}}_x\times\hat{\boldsymbol{k}}$, which is linear in $\hat{\boldsymbol{k}}$ and shows that for this special case, linear superposition of external flow and electrophoresis applies. Second, it is evident from Eq. (39a) that the second term on the r.h.s. denotes the contribution to the angular velocity from electrophoresis (namely, $\boldsymbol{\Omega}_0^E$), and this helps us identify the *electrophoresis-dominated scenario*, where $|\boldsymbol{\Omega}_0^E|/|\boldsymbol{\Omega}_0^\infty| > 1$, which

may be recast as $2\mathcal{R}_0 > 1$ or, $\alpha > \alpha_{\rm cr}$, where $\alpha_{\rm cr} = 2/9H^{(1)}$. Although it is perhaps obvious that electrophoresis will start dominating over the imposed flow as α is increased, the above argument nevertheless helps us pinpoint the critical value of α where this transition occurs. Conversely, when $\alpha < \alpha_{\rm cr}$, the externally imposed flow dominates the motion of the particle; in what follows, this case is referred to as the *flow-dominated scenario*. We further note that $\alpha_{\rm cr}$ is not a universal constant and depends on the dipole moment of the particle's surface charge distribution.

It is rather straightforward to deduce the fixed points [66] of Eq. (39a), from which further insights may be gained. When $\alpha < \alpha_{\rm cr}$ (flow-dominated scenario), there are two fixed points in Eq. (39a), given by $(\pm\sqrt{1-4\mathcal{R}_0^2}, -2\mathcal{R}_0, 0)$. It may be shown that the eigenvalues at both of these fixed points ($\gamma_\pm^\infty$, say) are purely imaginary (indeed, we find $\gamma_\pm^\infty = \pm\frac{i}{2}\sqrt{1-4\mathcal{R}_0^2}$), which indicates that these are possibly *centers* [66]. Although as fixed points, centers are delicate objects, noting that in Eq. (39a) the quantity $|\hat{\boldsymbol{k}}(t)|^2 = \hat{k}_x^2 + \hat{k}_y^2 + \hat{k}_z^2 = 1$ is conserved, it may be concluded that the two fixed points mentioned above are indeed *nonlinear centers* [66], as also confirmed by the numerical simulations discussed ahead. As a consequence, we infer that in the $\hat{k}_x - \hat{k}_y - \hat{k}_z$ phase space, $\hat{\boldsymbol{k}}(t)$ follows closed orbits around one of the two fixed points depending on the initial condition. Physically, this implies that the vector $\hat{\boldsymbol{k}}$ oscillates around the vector $\pm\sqrt{1-4\mathcal{R}_0^2}\hat{\mathbf{e}}_x - 2\mathcal{R}_0\hat{\mathbf{e}}_y$ when viewed w.r.t. the central axis. In other words, in the flow-dominated scenario, the particle will continually rotate around the vector(s) $\pm\sqrt{1-4\mathcal{R}_0^2}\hat{\mathbf{e}}_x - 2\mathcal{R}_0\hat{\mathbf{e}}_y$, and its angular velocity itself will also oscillate in time because the electrophoretic torque on the particle is not sufficiently strong to balance the torque from the external flow. As a result, generally speaking, $\mathbf{H}^{(1)}$, $\mathbf{H}^{(2)}$, and $\boldsymbol{\mathcal{U}}_0$ all will continually vary with time. At the same time, it may be verified that Eq. (39b) has no fixed points, which further establishes that the particle's orientation never comes to a steady state in the flow-dominated scenario.

Conversely, for $\alpha > \alpha_{\rm cr}$ (electrophoresis-dominated scenario), the fixed points of $\hat{\boldsymbol{k}}$ are $(0, -\frac{1}{2\mathcal{R}_0}, \pm\sqrt{1-\frac{1}{4\mathcal{R}_0^2}})$. By evaluating the eigenvalues (say, $\gamma_\pm^{\rm E}$) at these two points, it may be shown that the first of the two fixed points is a stable node [66] (with $\gamma_+^{\rm E} = -\mathcal{R}_0\sqrt{1-\frac{1}{4\mathcal{R}_0^2}}, -2\mathcal{R}_0\sqrt{1-\frac{1}{4\mathcal{R}_0^2}}$) and the second one is unstable ($\gamma_-^{\rm E} = \mathcal{R}_0\sqrt{1-\frac{1}{4\mathcal{R}_0^2}}$, $2\mathcal{R}_0\sqrt{1-\frac{1}{4\mathcal{R}_0^2}}$). Hence, for $\alpha > \alpha_{\rm cr}$, all orbits in the $\hat{k}_x - \hat{k}_y - \hat{k}_z$ phase space eventually approach the first fixed point. At the same time, it is straightforward to show that the fixed points for $\hat{\boldsymbol{j}}$ in Eq. (39b) are degenerate (but stable) in nature, and hence the ultimate (fixed) state of $\hat{\boldsymbol{j}}$ will depend on how it was initially oriented. Physically, this means that after an initial transience, the body-fixed unit vector $\hat{\boldsymbol{k}}$ will point in the direction $-(2\mathcal{R}_0)^{-1}\hat{\mathbf{e}}_y + \sqrt{1-(4\mathcal{R}_0)^{-2}}\hat{\mathbf{e}}_z$ and the particle will stop rotating after this alignment occurs. In other words, in the electrophoresis-dominated scenario, the torque on the particle due to the electric field balances that from the external flow, because of which the particle's rotation eventually stops, and from this point onwards, its cross-stream migration velocities (if any) along with the multipole moments also become steady. The above discussion thus highlights that depending on whether electrophoresis or the external flow is dominant, a particle's rotational motion and its orientation can exhibit qualitatively very different behavior.

Figure 2 illustrates the orbits (or, integral paths) of $\hat{\boldsymbol{k}}(t)$ in the $\hat{k}_x - \hat{k}_y - \hat{k}_z$ phase space for the electrophoresis-dominated [Fig. 2(a)] and the flow-dominated [Fig. 2(b)] scenarios. The surface charge distribution has been chosen as $\breve{\zeta}(\eta, \bar{\phi}, ; t = 0) = 1 - \sqrt{1-\eta^2}\sin\bar{\phi}$. The integral paths in the figure have been constructed by solving Eq. (39a) numerically using a fourth-order Runge-Kutta method. It may be verified that for the specific choice of $\breve{\zeta}$ mentioned as above, $H^{(1)} = 0.333$, $\alpha_{\rm cr} = 0.667$, while $H_{mn}^{(2)} = 0$, $\forall\, m,\ n$. As such, we have chosen $\alpha = 0.4 < \alpha_{\rm cr}$ in Fig. 2(a) (and therefore, $\mathcal{R}_0 = 0.3$), while in Fig. 2(b), $\alpha = 1$ (and thus $\mathcal{R}_0 = 0.75$). The respective fixed points then become $(\pm 0.8, -0.6, 0)$ [Fig. 2(a)] and $(0, -0.667, \pm 0.7453)$ [Fig. 2(b)], all of which have been plotted in the figure as bold red dots. It is important to note here that because of the condition $\hat{k}_x^2 + \hat{k}_y^2 + \hat{k}_z^2 = 1$, all the orbits in the the $\hat{k}_x - \hat{k}_y - \hat{k}_z$ phase space will lie on the surface of a unit sphere centered at the origin, as also shown in the figure.

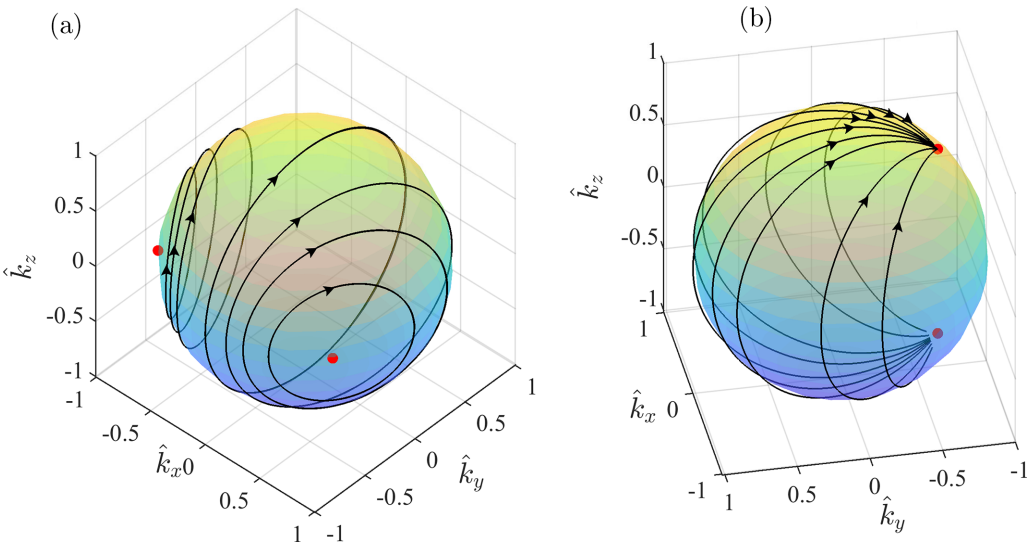

FIG. 2. Three-dimensional phase portraits of the body-fixed unit vector $\hat{\boldsymbol{k}}(t)$ for the flow-dominated scenario with $\alpha = 0.4 < \alpha_{\rm cr}$ (a) and the electrophoresis-dominated scenario with $\alpha = 1 > \alpha_{\rm cr}$ (b). We choose $\breve{\zeta}(\eta, \bar{\phi}; t = 0) = 1 - \sqrt{1-\eta^2}\sin\bar{\phi}$. The black lines indicate the integral paths of the unit vector $\hat{\boldsymbol{k}}$; the red dots are the fixed points corresponding to the two cases. All integral paths will lie on a unit sphere centered at the origin.

Indeed, when $\alpha < \alpha_{\rm cr}$, all the orbits are closed, indicating that $\hat{\boldsymbol{k}}(t)$ varies periodically and hence undergoes continuous oscillations. On the other hand, the existence of a stable fixed point is also evident in Fig. 2(b) as all the integral paths tend to move towards it (and away from the unstable fixed point) in time.

We end our discussion on rotational motion with a final note on the case of pure electrophoresis, which entails $\boldsymbol{\Omega}_\infty = 0$. Then Eq. (39a) simplifies to $d\hat{\boldsymbol{k}}/dt = \mathcal{R}_0(\hat{\boldsymbol{k}} \times \hat{\mathbf{e}}_z) \times \hat{\boldsymbol{k}}$, which has only two fixed points $(0, 0, \pm 1)$ with the first one being the stable one. Physically, it means that for pure electrophoretic motion, the particle will keep on rotating until its dipole moment points in the direction of the applied electric field, after which it stops rotating [67] and travels along a straight trajectory, as reported earlier in Ref. [8].

We now proceed to complete the reduced order model by evaluating the particle's trajectory, for which its linear velocity ($\boldsymbol{\mathcal{U}}_0$) first has to be estimated. To this end, we appeal to Eq. (38) and note that the particle's monopole (which is simply the net charge) is independent of its orientation, and thus it will be sufficient to compute the quadrupole moment $[\mathbf{H}^{(2)}(t)]$ associated with the zeta distribution $\breve{\zeta}(\bar{\theta}, \bar{\phi}; t)$ as a function of time in the central (or the laboratory-fixed) axis to have a complete knowledge of the particle's velocity.

We would like to clarify that the components of $\mathbf{H}^{(1)}(t)$ and $\mathbf{H}^{(2)}(t)$ evaluated in the central axis continually vary in time because the surface charge also varies when viewed w.r.t. to this axis owing to the particle's rotation. On the other hand, in the body-fixed axis, all components of $\mathbf{H}^{(2)}$ (and also $\mathbf{H}^{(1)}$) remain invariant in time, and as a result the quadrupole moment may be expressed as $\mathbf{H}^{(2)} = \tilde{H}^{(2)}_{mn}\hat{\mathbf{f}}_m\hat{\mathbf{f}}_n$ (the Einstein summation rule has been followed here), where $\hat{\mathbf{f}}_m \equiv \hat{\boldsymbol{\imath}}$ when $m = 1$, $\hat{\mathbf{f}}_m \equiv \hat{\boldsymbol{\jmath}}$ when $m = 2$ and $\hat{\mathbf{f}}_m \equiv \hat{\boldsymbol{k}}$ when $m = 3$ and $\tilde{H}^{(2)}_{mn}$'s are constants denoting the mnth component of $\mathbf{H}^{(2)}$ in the body-fixed axis. In the central (or the laboratory-fixed) axis, the quadrupole moment may then be written as

$$\mathbf{H}^{(2)} = H^{(2)}_{pq}(t)\hat{\mathbf{e}}_p\hat{\mathbf{e}}_q, \quad \text{where,} \quad H^{(2)}_{pq}(t) = \mathcal{M}_{pm}(t)\mathcal{M}_{qn}(t)\tilde{H}^{(2)}_{mn}. \tag{41}$$

In the above, $\hat{\mathbf{e}}_p \equiv \hat{\mathbf{e}}_x$, $\hat{\mathbf{e}}_y$ and $\hat{\mathbf{e}}_z$, respectively, for $p = 1,\ 2$, and 3; $\mathcal{M}_{pm}(t) = \hat{\mathbf{e}}_p \cdot \hat{\mathbf{f}}_m$ is the pmth component of the rotation tensor and is a function of time as $\hat{\mathbf{f}}_m$'s (or, $\hat{\boldsymbol{\imath}}$, $\hat{\boldsymbol{\jmath}}$ and $\hat{\boldsymbol{k}}$) vary with time in the laboratory-fixed axis. The rotation tensor ($\boldsymbol{\mathcal{M}}$) may be computed by solving for $\hat{\boldsymbol{\imath}}(t)$, $\hat{\boldsymbol{\jmath}}(t)$, and $\hat{\boldsymbol{k}}(t)$ using Eqs. (39). The electrophoretic component of the particle's velocity [$\boldsymbol{\mathcal{U}}_0^E(t)$] may now be trivially computed using Eq. (38), from which the total particle velocity in a Newtonian fluid may be evaluated as $\boldsymbol{\mathcal{U}}_0(t) = \boldsymbol{\mathcal{U}}_0^E(t) + \boldsymbol{\mathcal{U}}_0^\infty(t)$, where $\boldsymbol{\mathcal{U}}_0^\infty(t) = y_p(t)\hat{\mathbf{e}}_z$ is the contribution from the far-field flow. The trajectory of the particle may then be constructed in the laboratory-fixed axis by solving

$$\frac{d\mathbf{x}_P}{dt} = y_p(t)\hat{\mathbf{e}}_z + \alpha\left(H^{(0)}\mathbf{I} - \frac{1}{2}\mathbf{H}^{(2)}\right)\cdot\hat{\mathbf{e}}_z, \tag{42}$$

subject to $\mathbf{x}_P(0) = y_0\hat{\mathbf{e}}_y$. To summarize, the particle trajectories may be computed using Eq. (42), wherein $H^{(0)}$ is calculated from Eq. (37a), $\mathbf{H}^{(2)}$ is estimated from Eq. (41), and the rotation tensor $\boldsymbol{\mathcal{M}}$ appearing therein may be evaluated by tracking the unit vectors $\hat{\boldsymbol{\imath}}(t)$, $\hat{\boldsymbol{\jmath}}(t)$, and $\hat{\boldsymbol{k}}(t)$ using Eqs. (39). Finally, it is worth noting that the reduced order framework presented here is quite general and may also be applied to other kinds of imposed flows (such as the Poiseuille flow) with little modification.

2. Comparison of the reduced order model and the numerical simulations for Newtonian fluids

In an effort to assess the validity of the reduced order model, as an illustrative example, we consider the motion of a particle bearing a surface charge distribution, which has the following form at $t = 0$ in the central axis:

$$\breve{\zeta}(\eta, \bar{\phi}, t = 0) = 1 + \eta + \tfrac{1}{2}\sqrt{1-\eta^2}(\sin\bar{\phi} + \cos\bar{\phi})(1+\eta). \tag{43}$$

This particular charge distribution in so chosen as it bears a nonzero quadrupole moment $\mathbf{H}^{(2)}$, due to which we expect particle migration normal to the applied electric field even in a Newtonian medium. At the same time, the dipole moment resulting from the above charge distribution takes the form (at $t = 0$): $\mathbf{H}^{(1)} = 0.4082(0.4083\hat{\mathbf{e}}_x + 0.4083\hat{\mathbf{e}}_y + 0.8165\hat{\mathbf{e}}_z)$, where $|\mathbf{H}^{(1)}| = 0.4082$ and hence, at $t = 0$, $\hat{\boldsymbol{k}}(t = 0) = 0.4083\hat{\mathbf{e}}_x + 0.4083\hat{\mathbf{e}}_y + 0.8165\hat{\mathbf{e}}_z$. On the other hand, $\hat{\boldsymbol{\jmath}}$ is chosen as $\hat{\boldsymbol{\jmath}}(t = 0) = 0.9128\hat{\mathbf{e}}_x - 0.1826\hat{\mathbf{e}}_y - 0.3652\hat{\mathbf{e}}_z$, while $\hat{\boldsymbol{\imath}} = \hat{\boldsymbol{\jmath}} \times \hat{\boldsymbol{k}}$.

Figure 3 compares the results of the numerical simulation based on Sec. IV (with De = 0) and the reduced order model for the chosen surface charge distribution up to $t = 40$. Figures 3(a)–3(c), respectively, exhibit the temporal variations in the x, y and z components of $\boldsymbol{\mathcal{U}}_0$, while Figs. 3(d) and 3(e) portray the variations in the x and y components of $\boldsymbol{\Omega}_0$, respectively. Figure 3(f) depicts a direct comparison between the resulting particle trajectories, for $\alpha = 0.4 < \alpha_{\rm cr}$, with $\alpha_{\rm cr} = 0.544$ in the present case, which implies that Fig. 3 showcases particle motion in the flow-dominated scenario ($\alpha < \alpha_{\rm cr}$).

It is evident that the numerical simulations and the reduced order model show excellent agreement in all panels, thus underlining the accuracy of the latter. As noted in Sec. V A 1, in the flow-dominated scenario, the particle continuously rotates [see Figs. 3(d) and 3(e)], while the angular velocities themselves oscillate in time, and this results in the multipole moments periodically changing directions w.r.t. the applied electric field. As a consequence, the cross-stream migration velocities [see Figs. 3(a) and 3(b)] also undergo continuous oscillations in time, and this results in the particle continuously shifting between the negative and the positive halves of the xy plane. This has two interesting consequences; first, $\mathcal{U}_z$ also shows oscillatory behavior as the background flow periodically aids and opposes the electrophoretic motion; second, the resulting trajectory has a "spiraling" nature [see Fig. 3(f)], which prevents the particle from undergoing continuous cross-stream migration in any given direction. In the forthcoming subsection, we establish that similar trends are also observed when the suspending medium is viscoelastic, although the particle's overall tendency to migrate increases considerably in such complex fluids.

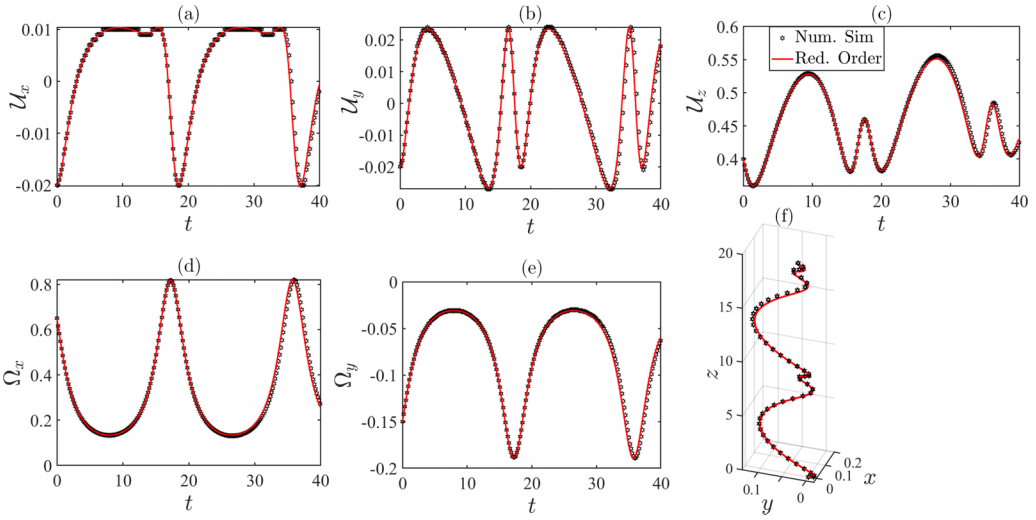

FIG. 3. Plot of the translational velocity components (a) $\mathcal{U}_x$, (b) $\mathcal{U}_y$, (c) $\mathcal{U}_z$, and the angular velocity components (d) Ω_x and (e) Ω_y for the same $\breve{\zeta}(\bar{\theta}, \bar{\phi}; t = 0)$ chosen in Eq. (43). The resulting particle trajectory is shown in (f). In all panels, the numerical simulations of Sec. IV B and the reduced order model of Sec. V A 1 have been compared. $\alpha = 0.4$.

B. Particle motion in viscoelastic fluids

1. Particles without any quadrupole moment ($H^{(2)}_{pq} = 0$)

As the first illustrative example, we consider the motion of a particle bearing an intrinsically axisymmetric charge represented in the laboratory-fixed (or the central) axis as follows:

$$\breve{\zeta}(\eta, \bar{\phi}; t = 0) = 1 - \sqrt{1 - \eta^2}\sin\bar{\phi}. \tag{44}$$

It is straightforward to verify that here $\mathbf{H}^{(1)} = 0.333\hat{\mathbf{e}}_y$ and thus initially, the dipole moment is not aligned with the direction of the applied electric field (as well as the flow). We emphasize that in this section, we shall follow the convention outlined in Fig. 1, wherein the central and the body-fixed axes coincide with each other at $t = 0$.

Figure 4 exhibits the resulting particle trajectories up to $t = 30$ for various choices of De $= 0$ (Newtonian), 0.05, 0.1, and 0.2, while the values of other relevant parameters have been mentioned

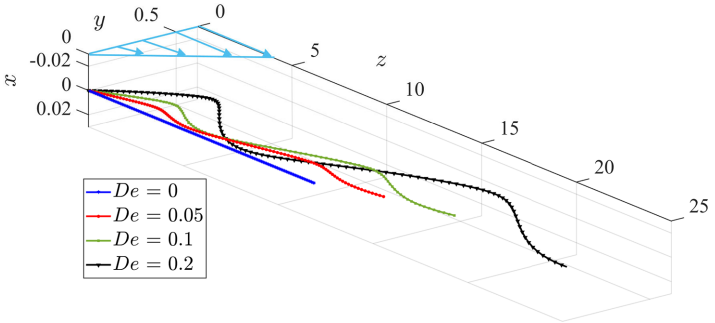

FIG. 4. Particle trajectories (up to $t = 30$ sec) for an initial surface charge distribution $\breve{\zeta}(\eta, \bar{\phi}; t = 0) = 1 - \sqrt{1 - \eta^2}\sin\bar{\phi}$ are shown for various choices of De $= 0$ (Newtonian), 0.05, 0.1, 0.2. $\alpha = 0.4$ ($< \alpha_{cr} = 0.667$), and $\lambda_2 = 0$. The light blue lines illustrate the imposed far-field linear flow (not to scale).

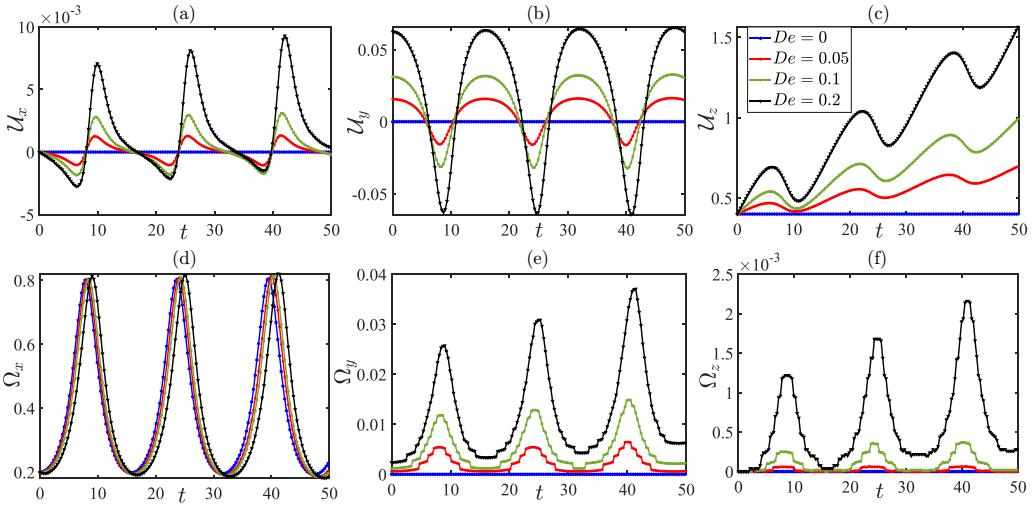

FIG. 5. Plot of the translational velocity components (a) $\mathcal{U}_x$, (*b*) $\mathcal{U}_y$, (c) $\mathcal{U}_z$, and the angular velocity components (d) Ω_x, (e) Ω_y, and (f) Ω_z of the particle as a function of time for De = 0, 0.05, 0.1, 0.2. All other parameters are identical to Fig. 4.

in the caption. The velocity field of the far-field external flow has also been shown (although this is not to scale) in this figure, and we have chosen $\alpha = 0.4 < \alpha_{\rm cr}(= 0.667)$, indicating that the motion is flow-dominated. Figure 5 illustrates the associated temporal variations in the translational and rotational velocities of the particle with time [the x, y, and z components of $\boldsymbol{\mathcal{U}}(t)$ respectively in Figs. 5(a)–5(c), and the x, y, and z components of $\boldsymbol{\Omega}(t)$ respectively in Figs. 5(d)–5(f)] for the scenario considered in Fig. 4.

Figure 4 shows that in a Newtonian medium (De = 0), the particle moves in a straight line along the direction of the applied electric field, simply because it does not possess any net quadrupole moment which can propel its cross-stream migration normal to the direction of the applied field [in Eq. (42), $\mathbf{H}^{(2)} = 0$]. This is corroborated by Fig. 5, wherein we observe that $\mathcal{U}_x$ and $\mathcal{U}_y$ are indeed zero when De = 0. Concomitantly, as expected in the flow-dominated scenario based on the discussion in Sec. V A 1, the particle undergoes continuous rotation around the x axis (only Ω_x is nonzero), although this rotation does not have any influence on its trajectory.

However, for De > 0, we do witness particle migration normal to applied electric field (primarily along the y direction), as also confirmed by Fig. 5, where both $\mathcal{U}_x$ and $\mathcal{U}_y$ become nonzero. The extent and the direction of migration as well as the distance traversed along the z direction strongly depends on the strength of viscoelasticity of the suspending medium, quantified by $\mathrm{De} = G\lambda_1'$. From Figs. 5(d)–5(f) we observe that akin to Newtonian fluids, the particle undergoes continuous rotation in viscoelastic fluids as well. This implies that although the reduced order model derived earlier does not directly apply here, the general features of the electrophoresis-dominated and the flow-dominated scenarios do remain valid for viscoelastic fluids, at least in the limit of weak viscoelasticity. At the same time now, Ω_y and Ω_z also become nonzero, which signals that the viscoelasticity of the medium changes the direction of the particle's rotation. In particular, nonzero Ω_z is rather rare in Newtonian fluids (for electric fields applied along the z direction) and is caused by the spontaneous breaking of fore-aft symmetry in viscoelastic media for nonuniformly charged particles [7].

From Figs. 5(a) and 5(b) we further observe that the cross-stream velocities oscillate in time, which causes the particle to shuttle back and forth in the xy plane. This explains the "oscillatory" nature of the trajectories shown in Fig. 4. On the other hand, any migration along the y direction will enhance the axial (i.e., the z component) velocity of the particle owing to the imposed flow

by increasing the offset distance [see, for instance, Eq. (31a)]. However, the oscillatory nature of $\mathcal{U}_y$ implies that the offset distance that the particle witnesses also varies periodically in time, which explains the oscillations seen in $\mathcal{U}_z$ in Fig. 5(c). From Fig. 5(b) we note that $\int_0^{\mathbb{T}} dt\mathcal{U}_y(t) > 0$ whenever De > 0, where $\mathbb{T}$ is the period of oscillation, which indicates net migration along the positive y axis and also explains the upward trend shown by $\mathcal{U}_z$ in Fig. 5(c).

The nonzero migration velocities ($\mathcal{U}_x$ and $\mathcal{U}_y$) originate from the interactions between the multipole moments (e.g., interactions between $\mathbf{H}^{(1)}$, $H^{(0)}$, and $\mathbf{E}_\infty$), along with the coupling between translation and rotation from the leading order, due to the nonlinear fluid constitution [8]. In case of pure electrophoretic motion of a particle with zero quadrupole moment, one observes an initial transient period during which the particle's dipole moment aligns itself along the applied electric field, which simultaneously causes the particle to rotate and undergo migration [8]. After the said alignment occurs, the particle stops rotating and moves along a straight trajectory in the direction of the applied field. However, in the presence of a background flow and especially in the flow-dominated scenario, the dipole moment of the particle undergoes continuous rotation and thus is unable to permanently orient itself along the imposed electric field. This keeps the interactions between the multipole moments along with the coupling between rotation and translation active at all times, and results in continuously nonzero cross stream migration velocities. As a consequence, despite having no quadrupole moment and carrying an intrinsically axisymmetric surface charge, the particle still undergoes cross-stream migration in viscoelastic fluids, albeit to a limited extent, which is otherwise not possible in a Newtonian medium. In fact, in Sec. III C 1 it has indeed been shown that presence of an imposed flow can lead to cross-stream migration, even when the particle carries an axisymmetric surface charge.

The oscillatory nature of $\mathcal{U}_x$ and $\mathcal{U}_y$ may be attributed to the fact that the direction of $\mathbf{H}^{(1)}$ (dipole moment) varies periodically because of the continuous rotation, and therefore the interactions between the multipole moments will also undergo periodic variations, which causes the cross-stream velocities to oscillate in time. Remarkably, Fig. 3 (and the reduced order model) also portrays a similar behavior of $\mathcal{U}_x$ and $\mathcal{U}_y$ in Newtonian fluids, albeit for a $\breve{\zeta}$ distribution with nonzero quadrupole moment, and this comes about primarily because of the periodic reorientations of $\mathbf{H}^{(1)}$ and $\mathbf{H}^{(2)}$, due to the particle's rotation. The same general features are also observed in viscoelastic medium, although now the nonlinear constitution of the fluid itself gives rise to additional interactions that increases the particle's propensity to undergo cross-stream migration.

2. Particles with nonzero quadrupole moments ($H^{(2)}_{pq} \neq 0$)

As a second representative example, we choose the same surface charge distribution considered in Sec. V A 2,

$$\breve{\zeta}(\eta, \bar{\phi}; t = 0) = 1 + \eta + \tfrac{1}{2}\sqrt{1-\eta^2}(\sin\bar{\phi} + \cos\bar{\phi})(1+\eta), \tag{45}$$

which bears a nonzero quadrupole moment $\mathbf{H}^{(2)}(t=0) = \frac{1}{10}(\hat{\mathbf{e}}_x\hat{\mathbf{e}}_z + \hat{\mathbf{e}}_y\hat{\mathbf{e}}_z)$ and therefore results in particle migration normal to the applied electric field in Newtonian fluids (De $= 0$) as well. Figure 6 depicts the resulting particle trajectories for various choices of De $= 0,\ 0.05,\ 0.1$, and 0.2 (the same as Fig. 4), and Fig. 7 showcases the temporal variations in the translational ($\mathcal{U}_x$, $\mathcal{U}_y$, and $\mathcal{U}_z$) and the angular velocity components (Ω_x, Ω_y, and Ω_z) of the particle during the course of its motion. The panelwise description of Fig. 7 is identical to that of Fig. 5. Furthermore, we have chosen $\alpha = 0.4 < \alpha_{\text{cr}}\ (= 0.544)$.

The overall trends shown by the trajectories as well as the velocity components of the particle remain unchanged from Figs. 4 and 5. Now the migration velocity components $\mathcal{U}_x$ and $\mathcal{U}_y$ are nonzero even when the surrounding medium is Newtonian (De $= 0$), due to the presence of a nonzero quadrupole moment. However, these migration velocities increase significantly as the medium becomes more viscoelastic, driven by the nonlinear interactions between the multipole moments, and the coupling between the angular and the translational velocities from the leading

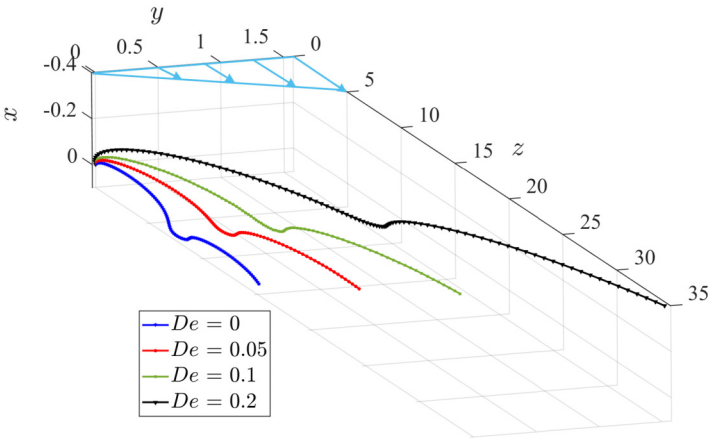

FIG. 6. Particle trajectories (up to $t = 30$ sec) for an initial surface charge distribution $\breve{\zeta}(\eta, \bar{\phi}; t = 0) = 1 + \eta + \frac{1}{2}\sqrt{1-\eta^2}(\sin\bar{\phi} + \cos\bar{\phi})(1+\eta)$ are shown for various choices of De $= 0$ (Newtonian), 0.05, 0.1, 0.2. Here $\alpha = 0.4 < \alpha_{cr}$ $(= 0.544)$. Other parameters are the same as in Fig. 4.

order, as noted in Sec. V B 1. Therefore, the extent of cross-stream migration is further enhanced in viscoelastic fluids, as evident from Fig. 6.

Akin to Fig. 4, because of the flow-dominated scenario being considered here (on account of $\alpha < \alpha_{\rm cr}$), the particle never ceases to rotate, as evident from Figs. 7(d)–7(f), while the viscoelasticity of the medium has little impact on its angular velocity (except Ω_z). This signals that the fundamental kinetics of rotation is still governed by the leading order interactions between the dipole moment, the electric field and the imposed flow, as discussed in Sec. V A 1. However, the medium's viscoelasticity is now seen to induce a significantly larger Ω_z as compared to the ones observed in Fig. 5 which is again caused by the breaking of fore-aft symmetry.

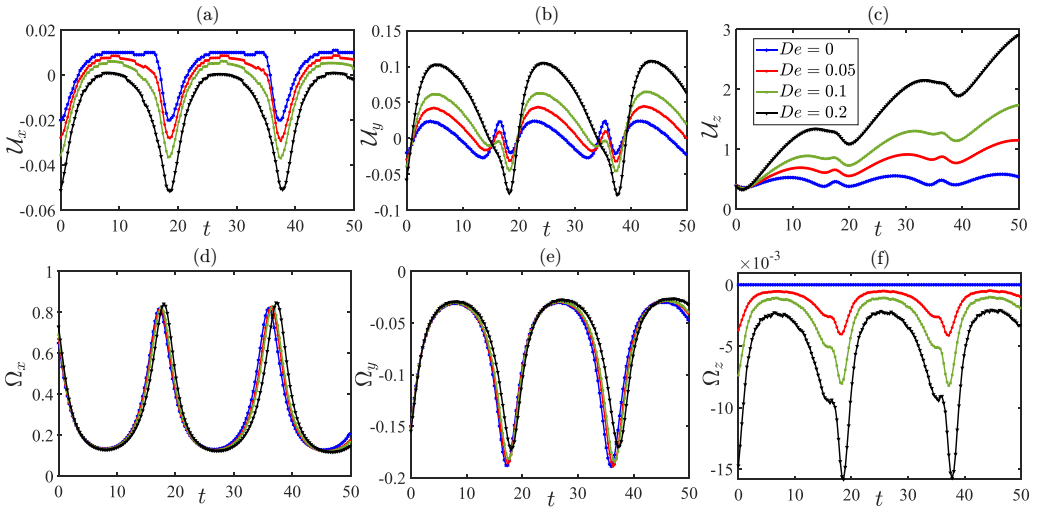

FIG. 7. Plot of the translational velocity components (a) $\mathcal{U}_x$, (b) $\mathcal{U}_y$, (c) $\mathcal{U}_z$, and the angular velocity components (d) Ω_x, (e) Ω_y, and (f) Ω_z of the particle as a function of time for De $= 0,\ 0.05,\ 0.1,\ 0.2$. All other parameters are identical to those in Fig. 6.

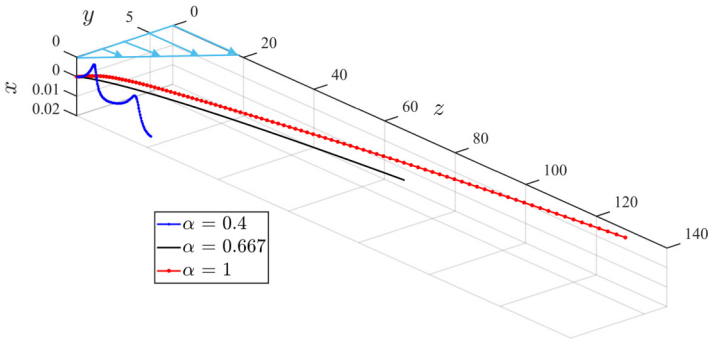

FIG. 8. Particle trajectories (up to $t = 30$ sec) for an initial surface charge distribution same as that of Fig. 4 are shown for various choices of $\alpha = 0.4$ ($< \alpha_{cr}$), $\alpha = 0.667 = \alpha_{cr}$, and $\alpha = 1$ ($> \alpha_{cr}$). We choose De $= 0.15$, while all other entities are same as that of 4.

3. Impact of α on particle trajectories

As the third representative example of our semianalytical framework, we explore the impact of α on the particle trajectories. Recall that the parameter α ($= u_E/u_S$) characterizes the strength of the electrophoretic velocity relative to the imposed shear flow. The previous discussion in Sec. V A establishes that in Newtonian fluids, the choice of α determines how the orientation of the particle evolves and hence will also strongly influence its trajectory. The same discussion also reveals the existence of a critical value of α (called α_{cr}), beyond which the transition between the flow-dominated and the electrophoresis-dominated scenarios occur. At the same time, the results from Secs. V B 1 and V B 2 show that the general features of particle motion (especially rotational motion) outlined in Sec. V A do remain valid in viscoelastic fluids as well, and hence similar transitions are also expected to occur therein.

We consider an initial surface charge distribution of the form (in the central axis)

$$\breve{\zeta}(\bar{\theta}, \bar{\phi}; t = 0) = 1 - \sqrt{1 - \eta^2} \sin \bar{\phi}, \tag{46}$$

which is identical to that in Fig. 4 and is intrinsically asymmetric in nature, with $\alpha_{cr} = 0.667$ (evaluated as per Sec. V A). Figure 8 illustrates the particle trajectories for three choices of $\alpha = 0.4 < \alpha_{cr}$ (the flow-dominated scenario), $\alpha = \alpha_{cr} = 0.667$ and $\alpha = 1 > \alpha_{cr}$ (electrophoresis-dominated scenario), while values of all other parameters have been mentioned in the caption. Figure 9 represents the associated temporal variations of the particle's velocity components, wherein the panelwise description remains identical to Fig. 5.

We observe from Fig. 8 that the nature of the particle's trajectory changes significantly, as its motion transitions from being flow-dominated ($\alpha < \alpha_{cr}$) to being electrophoresis-dominated ($\alpha > \alpha_{cr}$). For $\alpha = 0.4$ (flow-dominated scenario), the same trajectory as noted in Fig. 4 persists, which shows an oscillatory nature because of the continuous rotation of the particle; also see Figs. 9(d)–9(f). However, when electrophoresis dominates ($\alpha \gtrsim \alpha_{cr}$), the particle steadily migrates normal to the direction of the applied electric field, although now it stops rotating after an initial transience, as evident from those same panels. Hence, the particle's orientation eventually becomes stationary, which leads to steady-state migration velocities along the x and the y directions, as shown in Figs. 9(a) and 9(b). A steady $\mathcal{U}_y$ will enhance the offset distance at a fixed rate, which will cause $\mathcal{U}_z$ to increase linearly with time, as shown in Fig. 9(c). We further note that the migration velocities along the y direction ($\mathcal{U}_y$) have larger magnitudes in the electrophoresis-dominated scenario, and hence the extent of cross-stream migration is also expected to be larger, as is indeed observed in Fig. 8. The behavior described above for $\alpha > \alpha_{cr}$ is not surprising, given the discussions in Sec. V A 1, where it was shown that in the electrophoresis-dominated scenario, there exists a stable fixed point in the $\hat{k}_x - \hat{k}_y - \hat{k}_z$ phase space, and hence the dipole moment of the particle will finally

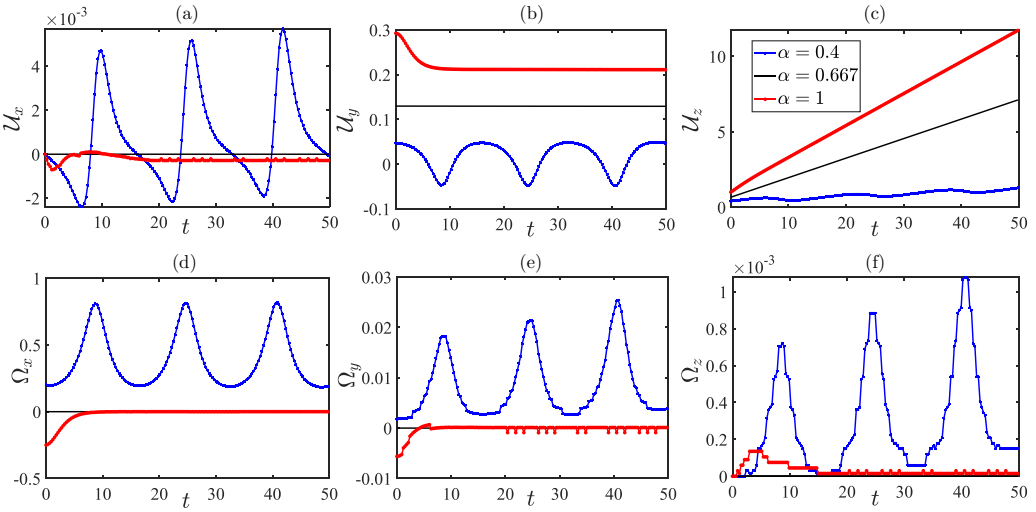

FIG. 9. Plot of the translational velocity components (a) $\mathcal{U}_x$, (b) $\mathcal{U}_y$, (c) $\mathcal{U}_z$, and the angular velocity components (d) Ω_x, (e) Ω_y, and (f) Ω_z of the particle as a function of time for various values of $\alpha = 0.4,\ 0.667$, and 1. All other entities are identical to those in Fig. 8.

be oriented in the direction of the said point (here at steady state, $\mathbf{H}^{(1)} = -0.2415\hat{\mathbf{e}}_y + 0.2299\hat{\mathbf{e}}_z$). Although the above conclusion was drawn only for Newtonian fluids, evidently it also applies to viscoelastic suspending medium as well, a feature that was also persistent throughout Secs. V B 1 and V B 2.

Perhaps the most striking feature of the trajectories shown in Fig. 8 is that even for particles without any quadrupole moment, we observe a steady state cross-stream migration, especially when $\alpha > \alpha_{cr}$. It has been previously shown [8] that for pure electrophoretic motion, a particle will only move along the direction of the applied electric field (no migration) at steady state if it carries no quadrupole moment. At the same time, no migrations occur in pure shear flows as well ($\alpha = 0$); see Sec. III C 2. Therefore, one may conclude that the steady cross-stream migration observed in Fig. 8 is a consequence of the interactions between the imposed shear flow and the electrophoretic motion, driven by the nonlinear constitution of the suspending medium.

4. General discussion on particle trajectories and their potential applications

It may now be possible to draw a few general conclusions based on the particle trajectories illustrated in the case studies of Secs. V B 1–V B 3. First, the very nature of a particle trajectory under the combined influence of an applied electric field and an imposed background flow depends on the relative dominance of these two actuating mechanisms. In general, a continuous trajectory is observed when the former dominates, while an oscillatory trajectory is seen when the latter dominates the particle motion. Second, it may be concluded that any particle in a viscoelastic medium will tend to undergo continuous migration (more so in the electrophoresis-dominated scenario) in the presence of an externally imposed flow, as long as it carries a nonuniform surface charge, which is sufficient to induce a nonzero dipole moment. However, if either of the two propelling forces (i.e., electric field or, external flow) is switched off, the cross-stream migration vanishes in the steady state. This is perhaps one of the most important features of particle motion, when electric field and background flow act in tandem in a viscoelastic medium. In contrast, in a Newtonian medium, the particle's surface charge density must have a nonzero quadrupole moment for it to undergo migration even in the presence of imposed flows, when $\mathrm{Re} \ll 1$.

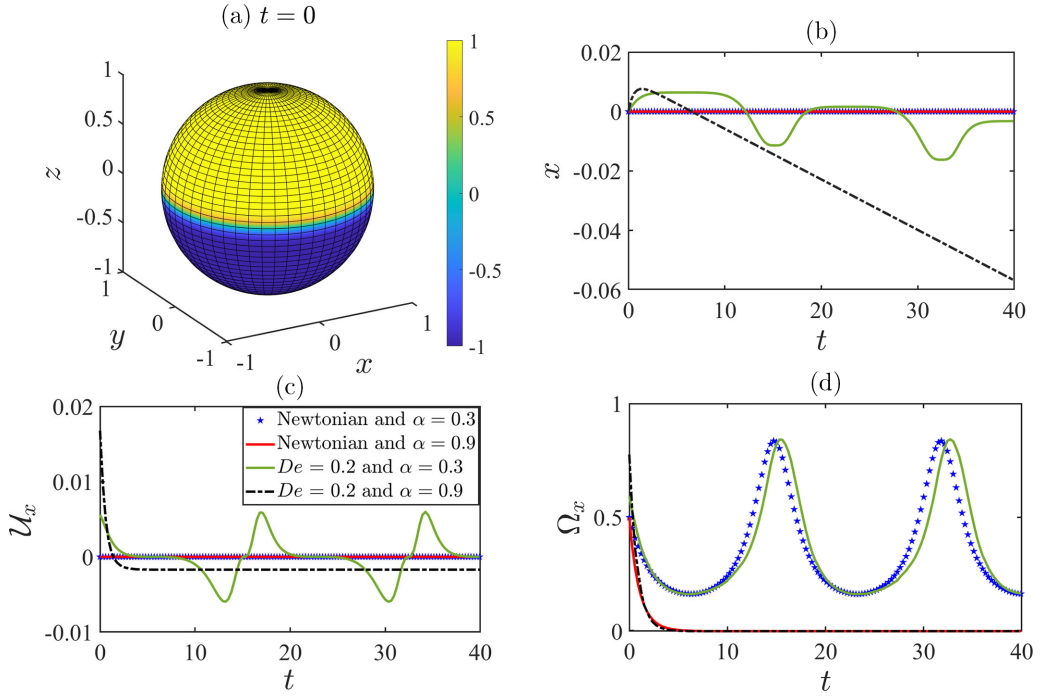

FIG. 10. (a) Initial ($t = 0$) $\breve{\zeta}(\eta, \bar{\phi})$ distribution of a Janus particle. (b) Variation in the x coordinate of the particle vs t till $t = 40$ in Newtonian (De = 0) and viscoelastic medium (De = 0.2), for $\alpha = 0.3 < \alpha_{\rm cr} = 0.4454$ and $\alpha = 0.9 > \alpha_{\rm cr}$. (c) $\mathcal{U}_x$ vs t and (d) Ω_x vs t for the motion shown in panel (b). All other parameters are identical to Fig. 4.

To test the above general observations, we carry out a final case study, where the trajectories of a Janus particle [68] are investigated. Usually the surface of such a particle is divided into two regions with distinct properties, e.g., charge density, which are represented by a discontinuous step function [68,69]. However such a description will not be suitable in regard to the present work as the O(De) slip velocities require the derivatives of $\breve{\zeta}$ with respect to η and $\bar{\phi}$, and a discontinuous $\breve{\zeta}$ would result in these derivatives blowing up. To overcome this issue, yet without compromising on the physical nature of a Janus particle, we choose the following surface charge distribution [8]:

$$\breve{\zeta}(\eta, \bar{\phi}, t = 0) = \tanh(\eta/0.05). \tag{47}$$

The "tanh" profile resolves the issue of discontinuity in $\breve{\zeta}$, while the relatively small width (0.05 in the polar direction) ensures a sharp variation across the particle surface. Equation (47) describes a particle carrying equal and opposite surface charge ($\breve{\zeta} = \pm 1$) on the two halves. Figure 10(a) exhibits this initial charge distribution. Note that the chosen $\breve{\zeta}$ is inherently axisymmetric, with zero net charge (equivalently, the monopole $H^{(0)} = 0$) and its quadrupole moment is also zero ($\mathbf{H}^{(2)} = \mathbf{0}$). Therefore, we expect that in a Newtonian fluid, the particle would rotate only without undergoing any net translation and cross-stream migration. Depending on the value of α, the particle's angular velocity may oscillate ($\alpha < \alpha_{\rm cr}$) or it may become completely standstill ($\alpha > \alpha_{\rm cr}$). On the other hand, based on the earlier assertions, it is expected that the particle will undergo some migration in a viscoelastic medium, since its surface charge is nonuniform, although it may not move along the z direction because of zero net charge.

Figure 10(b) portrays the variations in the x coordinate of the particle with time t for De = 0 (Newtonian) and De = 0.2 (viscoelastic). For each choice of De, we have separately considered

the flow-dominated ($\alpha = 0.3 < \alpha_{cr}$) and the electrophoresis-dominated scenarios ($\alpha = 0.9 > \alpha_{cr}$). Figures 10(c) and 10(d) respectively exhibit the associated translational and rotational velocities. It was found that for this particular scenario, the particle migrates along the x direction only when the medium is viscoelastic, which entails $\mathcal{U}_y(t) = \mathcal{U}_z(t) = \Omega_y(t) = \Omega_z(t) = 0$ at all times, and hence the variations in these quantities have not been shown.

It is evident from Figs. 10(c) and 10(d) that in a Newtonian medium the particle rotates without undergoing any translation. When $\alpha = 0.3$, Ω_x oscillates in time, whereas for $\alpha = 0.9$, it eventually reaches a steady state. In a viscoelastic medium also, the particle's angular motion shows very similar behavior, as observed in Fig. 10(d). However, from Fig. 10(c) one notes that despite carrying no net charge, the particle has a nonzero $\mathcal{U}_x$ only in a viscoelastic medium. When $\alpha = 0.3$, $\mathcal{U}_x$ undergoes oscillations akin to Ω_x, whereas for $\alpha = 0.9$, it quickly reaches a nonzero steady state value. The above results are nicely reflected in the particle's position in Fig. 10(b). In a Newtonian fluid, the particle does not move at all, while in a viscoelastic fluid, it undergoes either oscillatory or continuous migration along x, depending on the choice of α. The behavior of the particle described above is in complete agreement with our general observations laid out at the beginning of this subsection. We reiterate that the net migration observed in a viscoelastic fluid may be attributed to the breaking of fore-aft symmetry, forged out of the confluence between a nonuniform surface charge, an applied electric field and the imposed flow.

The generic features of the particle trajectories noted above may indeed find important applications in particle sorting and separation in micro- and millifluidic devices. To this end, it is worth emphasizing that $\alpha = u_E/u_S = \epsilon\zeta_c E_0/\mu G a$, which implies that $\alpha \sim 1/a$, where a is the particle size. Therefore, the various trajectories corresponding to varying α [see Figs. 8 and 10(b)] may also be interpreted as the path followed by particles of different sizes, everything else remaining the same. Larger particles will tend to have smaller α values, which signals that under identical external conditions, larger particles will tend to undergo flow-dominated motion, while the smaller ones will witness electrophoresis-dominated motion. Therefore, larger particles are more likely to follow oscillatory trajectories akin to the ones shown for $\alpha = 0.4$ in Fig. 8, while the smaller ones are likely to undergo continuous migration normal to the applied electric field.

It is important to note that any difference in the migration velocities along the y direction between two particles ($\Delta\mathcal{U}_y$, say) will result in the difference between their axial velocities (z components) grow as $\Delta\mathcal{U}_z \sim t$ because of the imposed flow and hence their axial separation will grow as $\Delta z \sim t^2$. Since $\mathcal{U}_y$ strongly depends on α and thereby on particle size, we may conclude that the above features of the particles' velocity differences may be useful in separating and sorting them according to their sizes, using a combination of externally controlled flow and electric field. While similar trends may also be possible in Newtonian fluids, the presence of a viscoelastic medium will undoubtedly improve the separation process, simply because any particle with a nonuniform surface charge is likely to undergo migration in such fluids.

In Newtonian medium, electrophoretic separation is usually achieved because particles with different charge-to-size ratios move with different velocities [14]. However, as per the leading order theory in the thin EDL limit, all particles move with the same velocity when they have identical surface charge density, irrespective of their sizes. In viscoelastic fluids on the other hand, a particle's velocity and its trajectory (when it is nonuniformly charged) will depend on its size, even in the thin EDL limit. This feature may potentially add another tool in our arsenal for separating and sorting particles based on their charge and size.

As a final note, we recall from recent studies [8] that particles of varying sizes carrying nonuniform surface charge tend to follow distinct trajectories (albeit of similar qualitative nature) in viscoelastic media. While this feature remains intact when externally imposed flows are present, the very nature of the trajectories may qualitatively change in such scenarios, depending on the particle size.

VI. EXPERIMENTAL PERSPECTIVES

A. Comparison with experimental studies

Li and Xuan [35] in an experimental study reported particle migration in viscoelastic fluids [aqueous polyethylene oxide (PEO) solution] in the presence of background flows. In an effort to compare our results with those of Li and Xuan, we refer to Sec. III C 1 where the electrophoretic velocity for a surface charge distribution of the form, $\breve{\zeta} = a_0 + a_{10}\eta$ was noted as (for simplicity, take $y_0 = 0$ and $\lambda_2 = 0$)

$$\boldsymbol{\mathcal{U}} = a_0\alpha\hat{\mathbf{e}}_z + \mathrm{De}\left(\tfrac{1}{20}\alpha a_{10}\hat{\mathbf{e}}_x - \tfrac{3}{5}\alpha^2 a_0 a_{10}\hat{\mathbf{e}}_z\right). \tag{48}$$

Now, for the special case of a uniformly charged particle (i.e., $a_0 = 1$ and $a_{10} = 0$), the electrophoretic velocity simplifies to $\boldsymbol{\mathcal{U}} = \alpha\hat{\mathbf{e}}_z + O(\mathrm{De}^2)$ as also reported earlier in Sec. III C 3. The dimensional form of this velocity reads $\boldsymbol{\mathcal{U}}' = u_E\,\hat{\mathbf{e}}_z$. Following the lead of Li and Xuan [35], we choose $\epsilon = 7 \times 10^{-10}$ F/m, $E_0 = 300$ V/cm, $\zeta_c = 50$ mV, and $\mu = 10^{-3}$ Pa s. This leads to $\boldsymbol{\mathcal{U}}' = 1.05\,\hat{\mathbf{e}}_z$ mm/s, which is of the same order as the experimentally reported magnitude of 0.36 mm/s. Note that Li and Xuan did not explicitly report the magnitude of the "zeta potential" (here ζ_c), and thus if we choose $\zeta_c \sim 20$ mV (the typical zeta potential of polystyrene particles used in the experiments are ∼20–200 mV [70]), we deduce $|\boldsymbol{\mathcal{U}}'| = 0.42$ mm/s, which is very close to experimentally measured value.

Since Li and Xuan [35] did not specify whether the particle's surface charge is uniform (which is unlikely), we now explore whether a small nonuniformity in it may predict the experimentally reported cross-stream migration. To this end, we choose $a_0 = 1$ and $a_{10} = 0.1$, such that $\breve{\zeta} = 1 + 0.1\eta$. The resulting particle velocity becomes (with units):

$$\boldsymbol{\mathcal{U}}' = \underbrace{\left(u_E - \frac{3}{50}\frac{u_E^2\lambda_1'}{a}\right)\hat{\mathbf{e}}_z}_{\boldsymbol{\mathcal{U}}'_{\mathrm{ax}}} + \underbrace{\frac{1}{200}\mathrm{De}\,u_E\hat{\mathbf{e}}_x}_{\boldsymbol{\mathcal{U}}'_{\mathrm{mig}}}. \tag{49}$$

From the work of Li and Xuan [35], we choose $a \sim 5$ μm, $\lambda_1' \sim 1.5$ ms. The Deborah number may be evaluated as $\mathrm{De} = u_S\lambda_1'/a = G'\lambda_1'$. For a volumetric flow rate of $Q' = 125$ μl/hr, and a channel dimension (width × depth) 50 μm × 100 μm, we deduce [35,46] $G' = 2Q'/w'^2d' \sim 277.77\ \mathrm{s}^{-1}$ and hence $\mathrm{De} = u_S\lambda_1'/a = 0.416$. Then, assuming $\zeta_c \sim 50$ mV, Eq. (49) yields $\boldsymbol{\mathcal{U}}' = 1.03 \times 10^{-3}\hat{\mathbf{e}}_z + 2.18 \times 10^{-6}\hat{\mathbf{e}}_x$ m/s. It thus follows that in principle, even a small nonuniformity in the surface charge of the simplest form can explain the observed cross-stream migration. It may be further noted that if we choose the length of the microchannel to be $L' = 2$ cm and the average fluid velocity $V'_{\mathrm{flow}} = 6.9$ mm/s [35], the residence time is estimated as $t'_{\mathrm{res}} \sim L'/(\boldsymbol{\mathcal{U}}'_{\mathrm{ax}} + V'_{\mathrm{flow}}) \sim 2.53$ s. Hence for the calculated migration velocity $\boldsymbol{\mathcal{U}}'_{\mathrm{mig}} = 2.18 \times 10^{-6}$, the maximum extent of migration due to a 10% charge inhomogeneity turns out to be approximately 5.51 μm.

Lu *et al.* [71] also reported electrophoretic velocities with a similar order of magnitude (∼0.5 mm/s) for spherical polystyrene particles in a constricted microchannel in both Newtonian and viscoelastic medium (aqueous PEO solution). However, they witnessed unusual particle oscillations predominantly in viscoelastic fluids, when their size increased beyond a threshold. Although the authors did not report the precise reason behind these oscillations, they argued that the possible reason might be either due to the formation of negative wakes downstream of the particles [71] or the formation and break-up of flow-induced structures [71]. Neither of these effects has been considered in the current work, and hence they are not expected to predict the occurrence of such oscillations.

B. A prospective experimental setup to test the present theory

We end our discussion with a brief outline of a prospective experimental setup that could be used to test some of our findings. A prototypical setup would consist of a capillary connected to two fluidic reservoirs at the ends. Electrodes may be placed within the reservoirs to impose the

TABLE III. Estimated range of values of various parameters that are relevant to a prospective experimental setup. Data taken from [8,35,37,71].

Physical parameters	Range of values
Size of polystyrene beads	1–10 μm
External electric field	100–400 V/cm
Concentration of PEO solution	50–1000 ppm
Zeta potential of the beads	10–200 mV
Length of the channel	1–4 cm
Channel dimension	200 μm × 200 μm
Flow rate	50–500 μl/hr
Electrophoretic axial velocity	$\sim 10^{-3}$–10^{-4} m/s
Electrophoretic migration velocity	$\sim 10^{-6}$–10^{-5} m/s

external electric field. Polystyrene spheres may be used as particles in an aqueous PEO solution, which is a viscoelastic medium with $\lambda_1' \sim 5$ ms and $\mu_0 \sim 1.5$ mPa s (zero-shear viscosity). The typical range of the relevant experimental parameters and the expected particle velocities have been included in Table III. A uniform pressure gradient may be applied to impose the external flow. The channel dimensions have been chosen to be sufficiently large such that the wall effects may be ignored. At the same time, a relatively small particle concentration should be used so that their interactions do not influence the results. The resulting trajectories may be tracked with the help of an inverted microscope equipped with a recording device, similar to the one reported in Ref. [35].

Finally, we would like to highlight some of the general predictions of our analysis that could be tested using the proposed experimental setup. First, particles of different sizes carrying the same surface charge profile should follow distinct trajectories. Smaller particles are expected to undergo continuous migration (electrophoresis-dominated motion), while the larger ones should traverse "oscillatory" trajectories (flow-dominated motion). Second, for a specific type of particle (same size and charge profile), the nature of its trajectory may be tuned by controlling the imposed electric field. The extent of migration should also become more prominent with increasing viscoelasticity (i.e., increase PEO concentration). Third, in Sec. III C 2 we observed that the viscoelastic medium has no effect on the particle's motion when $\alpha = 0$ (no electric field). It is only the presence of an electric field that results in the breaking of symmetry and eventual particle migration. Therefore, imposition of the external electric field should increase the suspended particles' propensity to undergo cross-stream migration.

VII. CONCLUSION

In this article we develop a general semianalytical framework to probe the electrophoretic motion of nonuniformly charged spherical particles in a viscoelastic medium in the presence of externally imposed linear (shear) flows. The particle is assumed to carry weak but otherwise arbitrary surface charge, the EDL surrounding it is assumed to be thin, while the viscoelastic effects are assumed to be subdominant. We use a combination of singular and regular perturbation to derive expressions of the modified Smoluchowski slip velocity and subsequently combine it with the Lamb's general solution and the reciprocal theorem to compute the resulting particle velocities. In general, the particle undergoes both translational and rotational motion, which transforms its surface charge distribution w.r.t. a laboratory-fixed axis during the course of its motion. This evolving charge distribution is computed by tracking a pair of unit vectors attached to the particle, and this knowledge of the particle's orientation is subsequently used to construct its trajectory. Our semianalytical framework is verified by considering a few specific instances of the surface charge distributions for which the particle velocities have been reported in the existing literature. We go on to extend the framework

and show that for the special case of Newtonian medium, the particle trajectories may be determined by solving a set of ordinary differential equations without any detailed knowledge of either the flow field or the surface charge distribution. As illustrative examples, we finally apply our framework to concoct particle trajectories in viscoelastic fluids for a few specific choices of initial surface charge distributions that offer useful insights into some generic features of particle motion.

We report several interesting conclusions from our current analysis. First, we show that in stark contrast to Newtonian fluids, the Smoluchowski slip velocity in a viscoelastic medium depends on the external flow (albeit indirectly) through the rotational motion it induces, which essentially stems from the vorticity of the imposed velocity field. Second, the reduced order model developed for particle motion in Newtonian fluids reveals that the particle's rotational motion and thereby to a large extent its trajectory is governed by the dominant propelling force. In the electrophoresis-dominated scenario, the particle eventually stops rotating, and its dipole orients in such a way that the torque due to the electric field and the external flow balance each other in a stable equilibrium. On the other hand, in the flow-dominated scenario, the torque due to electrophoresis is not sufficiently strong to balance the torque from the imposed flow because of which the particle continuously rotates. The transition from the flow-dominated to the electrophoresis-dominated scenario occurs when the parameter $\alpha > \alpha_{\mathrm{cr}}$, where α_{cr} is a constant and depends on the dipole moment of the particle's surface charge. The reduced order model further demonstrates that even in Newtonian fluids, a nonuniformly charge particle's trajectory can not be determined by linearly superimposing the individual effects of the background flow and electrophoretic motion. We go on to show that although the reduced order model does not quantitatively apply to viscoelastic fluids, the general features described above nevertheless remain applicable to such fluids, at least in the limit of weak viscoelasticity.

Third, it is established in the flow-dominated scenario, the particle trajectories tend to have an oscillatory nature with net cross-stream migration in viscoelastic fluids. In fact, we show that any particle with a nonuniform surface charge (regardless of the quadrupole moment) will undergo continuous migration in a viscoelastic fluid, when an externally imposed flow is present, and the reason for this is attributed to the interactions between the multipole moments and the imposed flow because of the nonlinear constitution of the fluid itself. It is further demonstrated that the extent of migration is larger when the particles carry a nonzero quadrupole moment. In the electrophoresis-dominated scenario, however, the particle attains a stationary orientation and thereby a steady migratory component of the velocity. This leads to a steady cross-stream migration, while the imposed flow quickly propels the particle forward. Again, these general characteristics may be observed whenever the particle carries a nonuniform surface charge.

Finally, we argue that under identical external conditions, larger particles tend to follow the flow-dominated scenario and smaller particles are more likely to follow the electrophoresis-dominated scenario, and thus they travel along qualitatively different trajectories. This may results in a quickly growing separation between particles of different sizes, which may be useful towards improving the separation processes using a confluence of electrophoretic actuation and imposed flow.

ACKNOWLEDGMENTS

R.B. acknowledges the Prime Minister's Research Fellowship (PMRF) for providing financial support for this work. U.G. is grateful to the Science and Engineering Research Board (SERB), Government of India, for providing financial support for this work through the MATRICS Grant No. MTR/2022/000365.

APPENDIX A: DERIVATION OF THE MODIFIED SMOLUCHOWSKI SLIP VELOCITY ($\mathbf{V}_{HS}$)

1. The inner layer equations

Following the discussion in Sec. II D 2, we deduce that in the thin EDL limit, the entire fluid domain may be divided into two regions, namely, an inner layer encompassing the EDL and the

TABLE IV. Rescaled variables within the inner layer.

Quantity	Scales as (within the inner layer)	Rescaled version
$u_{\bar{r}}$	$O(\delta)$	δV
$\varphi,\ c,\ \tilde{\rho}$	O(1)	$\Psi,\ C,\ \Pi$
$u_{\bar{\theta}},\ u_{\bar{\phi}},\ \tau_{\bar{r}\bar{r}},\ \mathcal{T}_{\bar{r}\bar{r}},\ \mathcal{S}_{\bar{r}\bar{r}}$	O(1)	$U, W, \check{\tau}_{\bar{r}\bar{r}}, \check{\mathcal{T}}_{\bar{r}\bar{r}}, \check{\mathcal{S}}_{\bar{r}\bar{r}}$
$D_{\bar{r}\bar{r}},\ D_{\bar{\theta}\bar{\theta}},\ D_{\bar{\theta}\bar{\phi}},\ D_{\bar{\phi}\bar{\phi}}$	O(1)	$\check{D}_{\bar{r}\bar{r}},\ \check{D}_{\bar{\theta}\bar{\theta}},\ \check{D}_{\bar{\theta}\bar{\phi}},\ \check{D}_{\bar{\phi}\bar{\phi}}$
$D_{\bar{r}\bar{\theta}},\ D_{\bar{r}\bar{\phi}}$	$O(\delta^{-1})$	$\delta^{-1}(\check{D}_{\bar{r}\bar{\theta}},\ \check{D}_{\bar{r}\bar{\phi}})$
$\tau_{\bar{r}\bar{\theta}},\ \tau_{\bar{r}\bar{\phi}},\ \mathcal{T}_{\bar{r}\bar{\theta}},\ \mathcal{T}_{\bar{r}\bar{\phi}}, \mathcal{S}_{\bar{r}\bar{\theta}},\ \mathcal{S}_{\bar{r}\bar{\phi}}$	$O(\delta^{-1})$	$\delta^{-1}(\check{\tau}_{\bar{r}\bar{\theta}},\ \check{\tau}_{\bar{r}\bar{\phi}},\ \check{\mathcal{T}}_{\bar{r}\bar{\theta}},\ \check{\mathcal{T}}_{\bar{r}\bar{\phi}},\ \check{\mathcal{S}}_{\bar{r}\bar{\theta}},\ \check{\mathcal{S}}_{\bar{r}\bar{\phi}})$
$\tau_{\bar{\theta}\bar{\theta}},\ \tau_{\bar{\theta}\bar{\phi}},\ \tau_{\bar{\phi}\bar{\phi}},\ p$	$O(\delta^{-2})$	$\delta^{-2}(\check{\tau}_{\bar{\theta}\bar{\theta}},\ \check{\tau}_{\bar{\theta}\bar{\phi}},\ \tau_{\bar{\phi}\bar{\phi}},\ P)$
$\mathcal{T}_{\bar{\theta}\bar{\theta}},\ \mathcal{T}_{\bar{\theta}\bar{\phi}},\ \mathcal{T}_{\bar{\phi}\bar{\phi}},\ \mathcal{S}_{\bar{\theta}\bar{\theta}},\ \mathcal{S}_{\bar{\theta}\bar{\phi}},\ \mathcal{S}_{\bar{\phi}\bar{\phi}}$	$O(\delta^{-2})$	$\delta^{-2}(\check{\mathcal{T}}_{\bar{\theta}\bar{\theta}},\ \check{\mathcal{T}}_{\bar{\theta}\bar{\phi}},\ \check{\mathcal{T}}_{\bar{\phi}\bar{\phi}},\ \check{\mathcal{S}}_{\bar{\theta}\bar{\theta}},\ \check{\mathcal{S}}_{\bar{\theta}\bar{\phi}},\ \check{\mathcal{S}}_{\bar{\phi}\bar{\phi}})$

outer layer or the bulk. Within the inner layer, the characteristic length scale is δ (i.e., $\bar{r}-1\sim\delta$), and hence appropriately rescaled versions of the governing equations must be derived within this region, which are then solved to deduce $\mathbf{V}_{HS}$ as outlined in Sec. II D 3. The flow within the EDL is better described by defining a relative velocity as follows: $\mathbf{u}=\mathbf{v}-\boldsymbol{\mathcal{U}}$, where $\mathbf{u}=u_{\bar{r}}\hat{\mathbf{e}}_{\bar{r}}+u_{\bar{\theta}}\hat{\mathbf{e}}_{\bar{\theta}}+u_{\bar{\phi}}\hat{\mathbf{e}}_{\bar{\phi}}$. The details of the rescaling may be found in the Ref. [7], and as such, here we shall present only a brief summary of the same. First, we rescale the $\bar{r}$ coordinate as $R=(\bar{r}-1)/\delta$, such that $R\sim O(1)$, when $\bar{r}-1\sim O(\delta)$. The rest of the rescaled variables within the inner layer have been outlined in Table IV. We clarify that these rescaled variables are expressed either with capital letters (such as, $U,\ V,\ \Psi$, etc.) or with a "breve" above (such as $\check{\tau}_{\bar{r}\bar{\theta}},\ \check{\mathcal{T}}_{\bar{r}\bar{r}}$, etc.). We may now enforce the above rescaled variables into Eqs. (1), apply the expansion in Eq. (5), and retain only the leading terms in δ. Furthermore, noting that in the weak surface charge limit, $\bar{\zeta}_0\ll 1$, $\rho\sim O(\bar{\zeta}_0)$, $\tilde{\rho}\sim O(1)$, $\Psi\sim O(1)$, $C\sim O(1)$, and $\Pi\sim O(1)$, this limit may be enforced by neglecting the $O(\bar{\zeta}_0)$ and higher order terms in the resulting equations. As such, the leading order equations (in δ) within the inner layer in the weak surface charge limit take the following form:

$$\frac{\partial^2\Psi}{\partial R^2}=-\frac{\Pi}{2};\quad \frac{\partial^2 C}{\partial R^2}=0\ \text{ and }\ \frac{\partial^2\Pi}{\partial R^2}+\frac{\partial}{\partial R}\left(C\frac{\partial\Psi}{\partial R}\right)=0, \tag{A1a}$$

$$\frac{\partial V}{\partial R}-\frac{\partial}{\partial\eta}(U\sqrt{1-\eta^2})+\frac{1}{\sqrt{1-\eta^2}}\frac{\partial W}{\partial\bar{\phi}}=0, \tag{A1b}$$

$$\sqrt{1-\eta^2}\frac{\partial P}{\partial\eta}+\frac{\partial\check{\tau}_{\bar{r}\bar{\theta}}}{\partial R}-\frac{\partial}{\partial\eta}(\check{\tau}_{\bar{\theta}\bar{\theta}}\sqrt{1-\eta^2})+\frac{1}{\sqrt{1-\eta^2}}\frac{\partial\check{\tau}_{\bar{\theta}\bar{\phi}}}{\partial\bar{\phi}}-\frac{\eta\check{\tau}_{\bar{\phi}\bar{\phi}}}{\sqrt{1-\eta^2}}+\frac{3\alpha}{2}\sqrt{1-\eta^2}\frac{\partial^2\Psi}{\partial R^2}=0, \tag{A1c}$$

$$\frac{\partial P}{\partial R}=0;\quad \frac{-1}{\sqrt{1-\eta^2}}\frac{\partial P}{\partial\bar{\phi}}+\frac{\partial\check{\tau}_{\bar{r}\bar{\phi}}}{\partial R}-\frac{\partial}{\partial\eta}(\check{\tau}_{\bar{\theta}\bar{\phi}}\sqrt{1-\eta^2})+\frac{1}{\sqrt{1-\eta^2}}\frac{\partial\check{\tau}_{\bar{\phi}\bar{\phi}}}{\partial\bar{\phi}}+\frac{\eta\check{\tau}_{\theta\bar{\phi}}}{\sqrt{1-\eta^2}}=0, \tag{A1d}$$

$$\check{\tau}_{ij}+\mathrm{De}\check{\mathcal{T}}_{ij}=2[\check{D}_{ij}+\lambda_2\mathrm{De}\check{\mathcal{S}}_{ij}],\quad \text{when}\ \ ij\equiv\bar{r}\bar{r},\bar{r}\bar{\theta},\bar{r}\bar{\phi}, \tag{A1e}$$

$$\check{\tau}_{ij}+\mathrm{De}\check{\mathcal{T}}_{ij}=2\lambda_2\mathrm{De}\check{\mathcal{S}}_{ij},\quad \text{when}\ \ ij\equiv\bar{\theta}\bar{\theta},\bar{\theta}\bar{\phi},\bar{\phi}\bar{\phi}. \tag{A1f}$$

The detailed expressions for $\check{\mathcal{T}}_{ij},\ \check{\mathcal{S}}_{ij}$, and $\check{D}_{ij}$ may be found in Ref. [8]. The above equations are subject to the following boundary conditions on the particle surface (at $R=0$; also see Eqs. (2)]:

$$\frac{\partial\Psi}{\partial R}=-\check{\zeta}(\bar{\theta},\bar{\phi});\quad \frac{\partial C}{\partial R}=\frac{\partial\Pi}{\partial R}+C\frac{\partial\Psi}{\partial R}=0, \tag{A2a}$$

$$U=\Omega_y\cos\bar{\phi}-\Omega_x\sin\bar{\phi},\quad V=0,\ \text{and}\ W=-(\Omega_x\cos\bar{\phi}+\Omega_y\sin\bar{\phi})\eta+\Omega_z\sqrt{1-\eta^2}. \tag{A2b}$$

We further require that U, W, C, Φ, and Π all remain bounded within the EDL, as $R \to \infty$. Evidently, all equations and boundary conditions in the inner layer have been expressed w.r.t. the central axis.

2. The modified Smoluchowski slip velocity

We note that within the EDL, Ψ, C, and Π are independent of the fluid medium and thereby De. To deduce them, we may solve Eq. (A1a), subject to (A2a) and the solutions are $\Psi = \breve{\zeta}(\bar{\theta}, \bar{\phi})e^{-R}$, $C = 2$, and $\Pi = -2\Psi$. The velocity field within the EDL may be derived by enforcing the asymptotic expansion (6) corresponding to $\mathrm{De} \ll 1$ in Eqs. (A1b)–(A1f). The orderwise solutions are given below.

a. The $O(\mathrm{De}^0)$ velocity field

In the leading order of De, $P_0 = 0$ and

$$U_0 = \frac{3}{2}\alpha\sqrt{1-\eta^2}\breve{\zeta}(\bar{\theta}, \bar{\phi})(1 - e^{-R}) + \Gamma_1, \quad W_0 = \chi_1, \text{ and } V_0 = 3\alpha\omega_{1,\eta}(1 - R - e^{-R}) - \omega_2 R, \tag{A3}$$

where the expressions for Γ_1, χ_1, ω_1, and ω_2 have already been outlined in Appendix A 2. The leading order slip velocity defined as $\mathbf{V}_{HS}^{(0)} = \lim_{R\to\infty}[U_0\hat{\mathbf{e}}_{\bar{\theta}} + W_0\hat{\mathbf{e}}_{\bar{\phi}}] - \boldsymbol{\Omega}_0 \times \hat{\mathbf{e}}_{\bar{r}}$ [see Eq. (7)], may now be estimated using Eq. (A3), which is identical to Eq. (9a).

b. The $O(\mathrm{De})$ velocity field

The $O(\mathrm{De})$ equations governing the flow inside the EDL may be deduced from Eqs. (A1b)–(A1f) using the expansion (6); see Ref. [7] for further details. It may be shown that at $O(\mathrm{De})$, $P_1 = 0$, while the $\bar{\theta}$ and the $\bar{\phi}$ components of the velocity field, which are of interest to us, take the following form:

$$U_1 = (1 - \lambda_2)\big[\mathcal{A}_1(R, \eta)\omega_1^2 + \mathcal{A}_2(R, \eta)\omega_1 + \mathcal{A}_3(R, \eta)\omega_{1,\eta} + \mathcal{A}_4(R, \eta)\omega_{1,\phi}\big] + \Gamma_2, \tag{A4a}$$

$$W_1 = \chi_2 + (1 - \lambda_2)\omega_3(U_0 - \Gamma_1), \tag{A4b}$$

where $\mathcal{A}_1(R, \eta) = \frac{9\eta\alpha^2}{2(1-\eta^2)^{3/2}}(e^{-2R} - 1)$, $\mathcal{A}_2(R, \eta) = \mathcal{A}_{21}\Gamma_1 + \mathcal{A}_{22}\omega_{1,\eta} + \mathcal{A}_{23}\omega_2$, $\mathcal{A}_{21} = \frac{3\alpha\eta(1-e^{-R})}{1-\eta^2}$, $\mathcal{A}_{22} = -\frac{9\alpha^2(3-3e^{-R}-Re^{-R})}{\sqrt{1-\eta^2}}$, $\mathcal{A}_{23} = -\frac{3\alpha(1-e^{-R})}{\sqrt{1-\eta^2}}$, $\mathcal{A}_3 = 3\alpha(1 - e^{-R})\Gamma_1$, $\mathcal{A}_4 = \frac{3\alpha(1-e^{-R})\chi_1}{1-\eta^2}$ and ω_3 has been defined after Eq. (9c). The $O(\mathrm{De})$ correction to the slip velocity defined as $\mathbf{V}_{HS}^{(1)} = \lim_{R\to\infty}[U_1\hat{\mathbf{e}}_{\bar{\theta}} + W_1\hat{\mathbf{e}}_{\bar{\phi}}] - \boldsymbol{\Omega}_1 \times \hat{\mathbf{e}}_{\bar{r}}$, may be evaluated from Eq. (A4) and is identical to Eqs. (9b) and (9c).

APPENDIX B: DETAILS ON THE COEFFICIENTS IN THE LAMB'S GENERAL SOLUTION

The harmonics $\mathcal{Q}$ and Λ of the Lamb's general solution appearing in (13) have the following expressions:

$$\mathcal{Q}_{-(n+1)} = \bar{r}^{-n-1}\sum_{l=0}^{n} P_n^l(\eta)(B_{\ln}\cos l\bar{\phi} + \tilde{B}_{\ln}\sin l\bar{\phi}), \tag{B1a}$$

$$\Lambda_{-(n+1)} = \bar{r}^{-n-1}\sum_{l=0}^{n} P_n^l(\eta)(C_{\ln}\cos l\bar{\phi} + \tilde{C}_{\ln}\sin l\bar{\phi}). \tag{B1b}$$

Recall that the boundary condition for $\mathbf{v}_{0(d)}$ on particle surface reads $\mathbf{v}_{0(d)}(\bar{r} = 1, \bar{\theta}, \bar{\phi}) = \boldsymbol{\mathcal{U}}_0 + \boldsymbol{\Omega}_0 \times \hat{\mathbf{e}}_r + \mathbf{V}_{HS}^{(0)} - \mathbf{v}_\infty(\bar{r} = 1, \bar{\theta}, \bar{\phi})$, while the surface charge distribution $[\bar{\zeta}_0(\eta, \bar{\phi})]$ may be expressed as $\breve{\zeta}(\bar{\theta}, \bar{\phi}) = \sum_{n=0}^{\infty}\mathcal{J}_n(\eta, \bar{\phi})$, where $\mathcal{J}_n$ is the surface harmonic of order n. Hence, in view

of Eq. (9a) $\mathbf{v}_{0(d)}(\bar{r}=1,\bar{\theta},\bar{\phi})$ may be recast in the following general form:

$$\mathbf{v}_{0(d)}(1,\bar{\theta},\bar{\phi}) = v_{\bar{r},0(d)}\hat{\mathbf{e}}_{\bar{r}} + v_{\bar{\theta},0(d)}\hat{\mathbf{e}}_{\bar{\theta}} + v_{\bar{\phi},0(d)}\hat{\mathbf{e}}_{\bar{\phi}} = \sum_{l=0}^{\infty}\{\mathbf{M}_l(\bar{\theta})\cos l\bar{\phi} + \tilde{\mathbf{M}}_l(\bar{\theta})\sin l\bar{\phi}\}, \tag{B2}$$

where $\mathbf{M}_l(\bar{\theta}) = D_l(\bar{\theta})\hat{\mathbf{e}}_{\bar{r}} + E_l(\bar{\theta})\hat{\mathbf{e}}_{\bar{\theta}} + F_l(\bar{\theta})\hat{\mathbf{e}}_{\bar{\phi}}$, $\tilde{\mathbf{M}}_l(\bar{\theta}) = \tilde{D}_l(\bar{\theta})\hat{\mathbf{e}}_{\bar{r}} + \tilde{E}_l(\bar{\theta})\hat{\mathbf{e}}_{\bar{\theta}} + \tilde{F}_l(\bar{\theta})\hat{\mathbf{e}}_{\bar{\phi}}$, and these will depend on the specific form of $\breve{\zeta}(\bar{\theta},\bar{\phi})$. The coefficients $A_{\ln}, \tilde{A}_{\ln}, B_{\ln}, C_{\ln}, \tilde{C}_{\ln}$ may then be evaluated using the following expressions [63]:

$$A_{\ln} = \frac{2n-1}{2}\frac{(2n+1)(n-l)!}{(n+1)(n+l)!}\int_{-1}^{1}\left\{nD_l + \frac{\partial}{\partial\eta}(E_l\sin\bar{\theta}) - \frac{l\tilde{F}_l}{\sin\bar{\theta}}\right\}P_n^l(\eta)\,d\eta, \tag{B3a}$$

$$\tilde{A}_{\ln} = \frac{2n-1}{2}\frac{(2n+1)(n-l)!}{(n+1)(n+l)!}\int_{-1}^{1}\left\{n\tilde{D}_l + \frac{\partial}{\partial\eta}(\tilde{E}_l\sin\bar{\theta}) + \frac{lF_l}{\sin\bar{\theta}}\right\}P_n^l(\eta)\,d\eta, \tag{B3b}$$

$$B_{\ln} = \frac{1}{4}\frac{(2n+1)(n-l)!}{(n+1)(n+l)!}\int_{-1}^{1}\left\{(n-2)D_l + \frac{\partial}{\partial\eta}(E_l\sin\bar{\theta}) - \frac{l\tilde{F}_l}{\sin\bar{\theta}}\right\}P_n^l(\eta)\,d\eta, \tag{B3c}$$

$$\tilde{B}_{\ln} = \frac{1}{4}\frac{(2n+1)(n-l)!}{(n+1)(n+l)!}\int_{-1}^{1}\left\{(n-2)\tilde{D}_l + \frac{\partial}{\partial\eta}(\tilde{E}_l\sin\bar{\theta}) + \frac{lF_l}{\sin\bar{\theta}}\right\}P_n^l(\eta)\,d\eta, \tag{B3d}$$

$$C_{\ln} = \frac{1}{2n}\frac{(2n+1)(n-l)!}{(n+1)(n+l)!}\int_{-1}^{1}\left\{-\frac{\partial}{\partial\eta}(F_l\sin\bar{\theta}) - \frac{l\tilde{E}_l}{\sin\bar{\theta}}\right\}P_n^l(\eta)\,d\eta, \tag{B3e}$$

$$\tilde{C}_{\ln} = \frac{1}{2n}\frac{(2n+1)(n-l)!}{(n+1)(n+l)!}\int_{-1}^{1}\left\{-\frac{\partial}{\partial\eta}(\tilde{F}_l\sin\bar{\theta}) + \frac{lE_l}{\sin\bar{\theta}}\right\}P_n^l(\eta)\,d\eta. \tag{B3f}$$

The leading order velocity components have the following expressions [63]:

$$\begin{aligned} v_{\bar{r},0(d)} = {} & \sum_{n=1}^{\infty}\sum_{l=0}^{n}\frac{(n+1)P_n^l(\eta)}{2(2n-1)\bar{r}^{n+2}}\{[A_{\ln}\bar{r}^2 - 2B_{\ln}(2n-1)]\cos l\bar{\phi} \\ & + [\tilde{A}_{\ln}\bar{r}^2 - 2\tilde{B}_{\ln}(2n-1)]\sin l\bar{\phi}\}, \end{aligned} \tag{B4a}$$

$$\begin{aligned} v_{\bar{\theta},0(d)} = {} & \sum_{n=1}^{\infty}\sum_{l=0}^{n}\frac{1}{2\bar{r}^n\sin\bar{\theta}}\left\{\sin^2\bar{\theta}\,\left[P_n^l(\eta)\right]'\left[\frac{n-2}{n(2n-1)}(A_{\ln}\cos l\bar{\phi} + \tilde{A}_{\ln}\sin l\bar{\phi})\right.\right. \\ & \left.\left. - \frac{2}{\bar{r}^2}(B_{\ln}\cos l\bar{\phi} + \tilde{B}_{\ln}\sin l\bar{\phi})\right] + \frac{2l}{\bar{r}}P_n^l(\eta)\left[\tilde{C}_{\ln}\cos(l\bar{\phi}) - C_{\ln}\sin l\bar{\phi}\right]\right\}, \end{aligned} \tag{B4b}$$

$$\begin{aligned} v_{\bar{\phi},0(d)} = {} & \sum_{n=1}^{\infty}\sum_{l=0}^{n}\frac{1}{2\bar{r}^n\sin\bar{\theta}}\left\{lP_n^l(\eta)\left[\frac{n-2}{n(2n-1)}(-\tilde{A}_{\ln}\cos l\bar{\phi} + A_{\ln}\sin l\bar{\phi})\right.\right. \\ & \left.\left. + \frac{2}{\bar{r}^2}(\tilde{B}_{\ln}\cos l\bar{\phi} - B_{\ln}\sin l\bar{\phi})\right] + \frac{2}{\bar{r}}\sin^2\bar{\theta}\,\left[P_n^l(\eta)\right]'(C_{\ln}\cos l\bar{\phi} + \tilde{C}_{\ln}\sin l\bar{\phi})\right\}. \end{aligned} \tag{B4c}$$

APPENDIX C: TIME STEP INDEPENDENCE STUDY FOR THE TRAJECTORY COMPUTATIONS

Figure 11 compares the results for the linear and angular velocities of the particle upto $t = 15$, computed using time steps $\Delta t = 0.01$ and 0.005, while all other entities remain the same as in Sec. V B 1. It is evident that lowering the time step below $\Delta t = 0.01$ does not change the results, and hence we have chosen $\Delta t = 0.01$ for all viscoelastic simulations reported in Sec. V B.

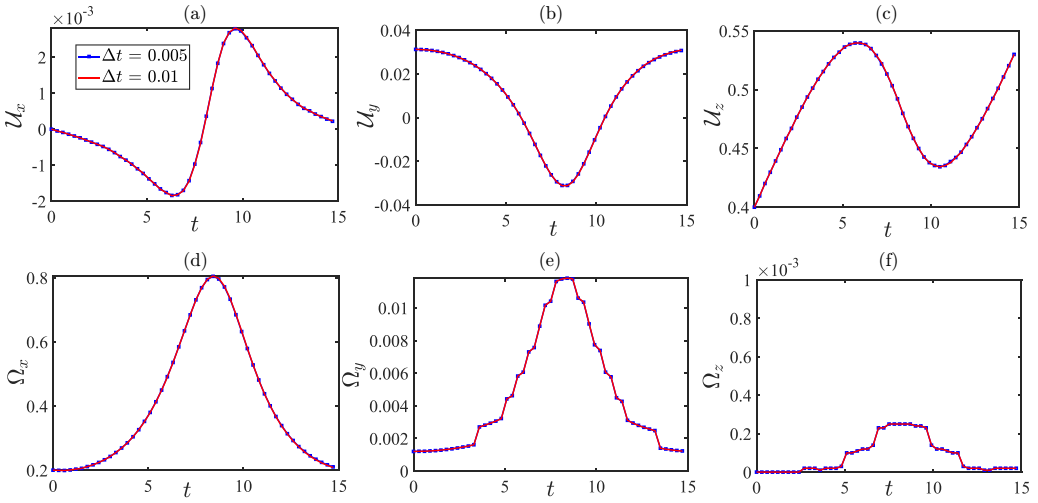

FIG. 11. Plot of the translational velocity components (a) $\mathcal{U}_x$, (b) $\mathcal{U}_y$, (c) $\mathcal{U}_z$, and the angular velocity components (d) Ω_x, (e) Ω_y, and (f) Ω_z of the particle as a function of time for two different time steps: $\Delta t = 0.01$ and $\Delta t = 0.005$. De $= 0.1$. All other entities are identical to Fig. 4.

[1] D. Saville, Electrokinetic effects with small particles, Annu. Rev. Fluid Mech. **9**, 321 (1977).

[2] J. L. Anderson, Effect of nonuniform zeta potential on particle movement in electric fields, J. Colloid Interface Sci. **105**, 45 (1985).

[3] H. Ohshima, Henry's function for electrophoresis of a cylindrical colloidal particle, J. Colloid Interface Sci. **180**, 299 (1996).

[4] H. Ohshima, *Theory of Colloid and Interfacial Phenomena* (Elsevier, 2006).

[5] O. Schnitzer, R. Zeyde, I. Yavneh, and E. Yariv, Weakly nonlinear electrophoresis of a highly charged colloidal particle, Phys. Fluids **25**, 052004 (2013).

[6] P. Goswami, J. Dhar, U. Ghosh, and S. Chakraborty, Solvent-mediated nonelectrostatic ion–ion interactions predicting anomalies in electrophoresis, Electrophoresis **38**, 712 (2017).

[7] U. Ghosh, S. Mukherjee, and S. Chakraborty, Electrophoretic motion of a nonuniformly charged particle in a viscoelastic medium in thin electrical double layer limit, J. Fluid Mech. **924**, A41 (2021).

[8] R. Borthakur and U. Ghosh, Electrophoretic trajectories of nonuniformly charged particles in viscoelastic fluids: The weak surface charge limit, J. Fluid Mech. **954**, A48 (2023).

[9] R. Cobos and A. S. Khair, Nonlinear electrophoretic velocity of a spherical colloidal particle, J. Fluid Mech. **968**, A14 (2023).

[10] A. S. Khair and T. M. Squires, The influence of hydrodynamic slip on the electrophoretic mobility of a spherical colloidal particle, Phys. Fluids **21**, 042001 (2009).

[11] A. Choudhary, T. Renganathan, and S. Pushpavanam, Inertial migration of an electrophoretic rigid sphere in a two-dimensional Poiseuille flow, J. Fluid Mech. **874**, 856 (2019).

[12] J. Sherwood and S. Ghosal, Electrophoresis of tightly fitting spheres along a circular cylinder of finite length, J. Fluid Mech. **929**, A45 (2021).

[13] S. Ghosal, Electrokinetic flow and dispersion in capillary electrophoresis, Annu. Rev. Fluid Mech. **38**, 309 (2006).

[14] R. Westermeier, *Electrophoresis in Practice: A Guide to Methods and Applications of DNA and Protein Separations* (Wiley-VCH, Weinheim, Germany, 2016).

[15] B. L. Karger, A. S. Cohen, and A. Guttman, High-performance capillary electrophoresis in the biological sciences, J. Chromatogr. B: Biomed. Sci. Appl. **492**, 585 (1989).
[16] G. Babnigg and C. S. Giometti, GELBANK: A database of annotated two-dimensional gel electrophoresis patterns of biological systems with completed genomes, Nucl. Acids Res. **32**, D582 (2004).
[17] L. Kremser, D. Blaas, and E. Kenndler, Capillary electrophoresis of biological particles: Viruses, bacteria, and eukaryotic cells, Electrophoresis **25**, 2282 (2004).
[18] R. Ramautar, A. Demirci, and G. J. de Jong, Capillary electrophoresis in metabolomics, Trends Anal. Chem. **25**, 455 (2006).
[19] Y.-W. Lin, T.-C. Chiu, and H.-T. Chang, Laser-induced fluorescence technique for DNA and proteins separated by capillary electrophoresis, J. Chromatogr. B **793**, 37 (2003).
[20] R. T. Turgeon and M. T. Bowser, Micro free-flow electrophoresis: Theory and applications, Anal. Bioanal. Chem. **394**, 187 (2009).
[21] D. Kohlheyer, J. C. Eijkel, A. van den Berg, and R. B. Schasfoort, Miniaturizing free-flow electrophoresis—A critical review, Electrophoresis **29**, 977 (2008).
[22] M. von Smoluchowski, Contribution à la théorie de l'endosmose électrique et de quelques phénomènes corrélatifs, Bull. Akad. Sci. Cracovie **8**, 182 (1903).
[23] P. J. W. Debye and E. Hückel, *Bemerkungen zu einem Satze über die kataphoretische Wanderungsgeschwindigkeit suspendierter Teilchen* (Hirzel, 1924).
[24] O. Schnitzer and E. Yariv, Strong-field electrophoresis, J. Fluid Mech. **701**, 333 (2012).
[25] J. J. López-García, J. Horno, and C. Grosse, Ionic size, permittivity, and viscosity-related effects on the electrophoretic mobility: A modified electrokinetic model, Phys. Rev. Fluids **4**, 103702 (2019).
[26] G. S. Ganchenko, E. A. Frants, V. S. Shelistov, N. V. Nikitin, S. Amiroudine, and E. A. Demekhin, Extreme nonequilibrium electrophoresis of an ion-selective microgranule, Phys. Rev. Fluids **4**, 043703 (2019).
[27] R. F. Stout and A. S. Khair, A continuum approach to predicting electrophoretic mobility reversals, J. Fluid Mech. **752**, R1 (2014).
[28] S. Ghosal, Electrophoresis of a polyelectrolyte through a nanopore, Phys. Rev. E **74**, 041901 (2006).
[29] M. Fair and J. Anderson, Electrophoresis of nonuniformly charged ellipsoidal particles, J. Colloid Interface Sci. **127**, 388 (1989).
[30] L. G. Leal, *Advanced Transport Phenomena: Fluid Mechanics and Convective Transport Processes* (Cambridge University Press, 2007).
[31] D. Velegol, Electrophoresis of randomly charged particles, Electrophoresis **23**, 2023 (2002).
[32] T. Y. Molotilin, V. Lobaskin, and O. I. Vinogradova, Electrophoresis of Janus particles: A molecular dynamics simulation study, J. Chem. Phys. **145**, 244704 (2016).
[33] S.-P. Fu, R. Ryham, B. Quaife, and Y.-N. Young, Effects of tunable hydrophobicity on the collective hydrodynamics of Janus particles under flows, Phys. Rev. Fluids **8**, 050501 (2023).
[34] A. S. Khair, D. E. Posluszny, and L. M. Walker, Coupling electrokinetics and rheology: Electrophoresis in non-Newtonian fluids, Phys. Rev. E **85**, 016320 (2012).
[35] D. Li and X. Xuan, Electrophoretic slip-tuned particle migration in microchannel viscoelastic fluid flows, Phys. Rev. Fluids **3**, 074202 (2018).
[36] G. Li and D. L. Koch, Electrophoresis in dilute polymer solutions, J. Fluid Mech. **884**, A9 (2020).
[37] A. Choudhary, D. Li, T. Renganathan, X. Xuan, and S. Pushpavanam, Electrokinetically enhanced cross-stream particle migration in viscoelastic flows, J. Fluid Mech. **898**, A20 (2020).
[38] U. Ghosh and S. Chakraborty, Electroosmosis of viscoelastic fluids over charge modulated surfaces in narrow confinements, Phys. Fluids **27**, 062004 (2015).
[39] S. Chakraborty, Dynamics of capillary flow of blood into a microfluidic channel, Lab Chip **5**, 421 (2005).
[40] K. Raj M., S. Bhattacharya, S. DasGupta, and S. Chakraborty, Collective dynamics of red blood cells on an *in vitro* microfluidic platform, Lab Chip **18**, 3939 (2018).
[41] Z.-G. Su, T.-F. Li, K. Luo, and H.-L. Yi, Nonlinear behavior of electrohydrodynamic flow in viscoelastic fluids, Phys. Rev. Fluids **6**, 093701 (2021).

[42] D.-L. Chen, Y. Zhang, X.-L. Gao, K. Luo, J. Wu, and H.-L. Yi, Electrohydrodynamic conduction phenomena of a viscoelastic dielectric fluid with electroelastic instability, Phys. Rev. Fluids **8**, 053702 (2023).
[43] D. Posluszny, Electrophoresis of colloidal particles in shear-thinning polymer solutions, Ph.D. thesis, Carnegie Mellon University, 2014.
[44] J.-P. Hsu and L.-H. Yeh, Effect of a charged boundary on electrophoresis in a carreau fluid: A sphere at an arbitrary position in a spherical cavity, Langmuir **23**, 8637 (2007).
[45] E. Lee, C.-T. Chen, and J.-P. Hsu, Electrophoresis of a rigid sphere in a Carreau fluid normal to a planar surface, J. Colloid Interface Sci. **285**, 857 (2005).
[46] A. S. Khair and J. K. Kabarowski, Migration of an electrophoretic particle in a weakly inertial or viscoelastic shear flow, Phys. Rev. Fluids **5**, 033702 (2020).
[47] A. Choudhary, T. Renganathan, and S. Pushpavanam, Comment on "migration of an electrophoretic particle in a weakly inertial or viscoelastic shear flow", Phys. Rev. Fluids **6**, 036701 (2021).
[48] R. B. Bird, R. C. Armstrong, and O. Hassager, *Dynamics of Polymeric Liquids, Vol. 1: Fluid Mechanics* (John Wiley and Sons, Hoboken, New Jersey, US, 1987).
[49] J. Happel and H. Brenner, *Low Reynolds Number Hydrodynamics: With Special Applications to Particulate Media* (Springer Science & Business Media, Berlin, Germany, 2012), Vol. 1.
[50] H. Masoud and H. A. Stone, The reciprocal theorem in fluid dynamics and transport phenomena, J. Fluid Mech. **879**, P1 (2019).
[51] C. Esparza López and E. Lauga, Rate invariance and scallop theorem in viscosity gradients, Phys. Rev. Fluids **8**, 063301 (2023).
[52] A. Ajdari, Generation of transverse fluid currents and forces by an electric field: Electro-osmosis on charge-modulated and undulated surfaces, Phys. Rev. E **53**, 4996 (1996).
[53] M. Mirzadeh, T. Zhou, M. A. Amooie, D. Fraggedakis, T. R. Ferguson, and M. Z. Bazant, Vortices of electro-osmotic flow in heterogeneous porous media, Phys. Rev. Fluids **5**, 103701 (2020).
[54] A. Ajdari, Electro-osmosis on inhomogeneously charged surfaces, Phys. Rev. Lett. **75**, 755 (1995).
[55] A. Afonso, M. Alves, and F. Pinho, Analytical solution of mixed electro-osmotic/pressure driven flows of viscoelastic fluids in microchannels, J. Non-Newtonian Fluid Mech. **159**, 50 (2009).
[56] B. Mahapatra and A. Bandopadhyay, Numerical analysis of combined electroosmotic-pressure driven flow of a viscoelastic fluid over high zeta potential modulated surfaces, Phys. Fluids **33**, 012001 (2021).
[57] O. Schnitzer and E. Yariv, Nonlinear electrophoresis at arbitrary field strengths: Small-Dukhin-number analysis, Phys. Fluids **26**, 122002 (2014).
[58] C. Ye, D. Sinton, D. Erickson, and D. Li, Electrophoretic motion of a circular cylindrical particle in a circular cylindrical microchannel, Langmuir **18**, 9095 (2002).
[59] G. Y. Chen and H. J. Keh, Start-up of electrophoresis of an arbitrarily oriented dielectric cylinder, Electrophoresis **35**, 2560 (2014).
[60] U. Ghosh, K. Chaudhury, and S. Chakraborty, Electroosmosis over non-uniformly charged surfaces: Modified Smoluchowski slip velocity for second-order fluids, J. Fluid Mech. **809**, 664 (2016).
[61] E. Yariv, An asymptotic derivation of the thin-debye-layer limit for electrokinetic phenomena, Chem. Eng. Commun. **197**, 3 (2009).
[62] E. Lauga, *The Fluid Dynamics of Cell Motility* (Cambridge University Press, 2020).
[63] O. S. Pak and E. Lauga, Generalized squirming motion of a sphere, J. Eng. Math. **88**, 1 (2014).
[64] C. Pozrikidis and D. Jankowski, *Introduction to Theoretical and Computational Fluid Dynamics* (Oxford University Press, New York, 1997), Vol. 675.
[65] A. Mozaffari, N. Sharifi-Mood, J. Koplik, and C. Maldarelli, Self-propelled colloidal particle near a planar wall: A Brownian dynamics study, Phys. Rev. Fluids **3**, 014104 (2018).
[66] S. H. Strogatz, *Nonlinear Dynamics and Chaos: With Applications to Physics, Biology, Chemistry, and Engineering* (CRC Press, 2018).
[67] D. J. Griffiths, *Introduction to Electrodynamics* (Prentice Hall, Hoboken, New Jersey, US, 1962).
[68] B. Nasouri and R. Golestanian, Exact axisymmetric interaction of phoretically active Janus particles, J. Fluid Mech. **905**, A13 (2020).
[69] P. Bayati and A. Najafi, Electrophoresis of active Janus particles, J. Chem. Phys. **150**, 234902 (2019).

[70] O. El-Gholabzouri, M. Á. Cabrerizo-Vílchez, and R. Hidalgo-Álvarez, Zeta-potential of polystyrene latex determined using different electrokinetic techniques in binary liquid mixtures, Colloids Surf. A **291**, 30 (2006).

[71] X. Lu, S. Patel, M. Zhang, S. Woo Joo, S. Qian, A. Ogale, and X. Xuan, An unexpected particle oscillation for electrophoresis in viscoelastic fluids through a microchannel constriction, Biomicrofluidics **8**, 021802 (2014).